HHS Public Access

Author manuscript

Math Biosci. Author manuscript; available in PMC 2019 February 25.

Published in final edited form as:

Math Biosci. 1994 March ; 120(1): 25–76.

A G Protein-Based Model of Adaptation in *Dictyostelium discoideum*

YUANHUA TANG and **HANS G. OTHMER**

Department of Mathematics, University of Utah, Salt Lake City, Utah 84112

Abstract

A new model is proposed based on signal transduction via G proteins for adaptation of the signal relay process in the cellular slime mold *Dictyostelium discoideum*. The kinetic constants involved in the model are estimated from *Dictyostelium discoideum* and other systems. A qualitative analysis of the model shows how adaptation arises, and numerical computations show that the model agrees with observations in both perfusion and suspension experiments. Several experiments that can serve to test the model are suggested.

1. INTRODUCTION

The cellular slime mold *Dictyostelium discoideum* (*Dd* hereafter) is a widely used system for the study of many developmental processes, including extracellular communication, signal transduction, chemotaxis, pattern formation, and differentiation [8]. In the presence of an adequate food supply the amoebas exist as free-ranging individuals, but when the food supply is exhausted an elaborate developmental program is initiated. After a period of starvation, cells attain relay competence, by which it is meant that they can detect an external cAMP pulse and respond to it by synthesizing and releasing cAMP. Experiments show that the response to cAMP has two separate components. One component is signal relay, which includes the adaptation of internal cAMP secretion to prolonged external cAMP stimuli. The other component includes cGMP synthesis and the effect of this on chemotaxis. Our objective here is to develop a new model for the cyclic AMP pathway and to explain how adaptation of the signal relay process occurs in this pathway. The cGMP pathway, which is linked to chemotaxis, is similar to the PI cycle found in mammalian cells [4, 15–17, 22]. Calcium is involved as a messenger in this pathway, and there appears to be some crosstalk between the chemotaxis-activating pathway and the signal relay pathway [41], but it is as yet not well enough defined to warrant detailed modeling.

There is a substantial body of experimental information on the input-output behavior of *Dd* under a variety of stimulus protocols [9–13], including short and prolonged stimuli and sequential stimuli. One important fact observed in these experiments is that the relay response adapts to constant stimuli over a range of four orders of magnitude in the stimulus amplitude. There are two components to relay adaptation: a rapid component that probably involves receptor modification and occurs on a time scale of minutes, and a slower component that involves down-regulation of receptors. Recent work on models of adaptation in signal relay are reported in [32]–[37], where an attempt was made to incorporate as many of the biochemical steps as possible. The two main biochemical pathways involved in the

models are activation of adenylate cyclase via a simplified transduction scheme in which the enzyme and receptor are precoupled, and an inhibitory pathway in which calcium regulates the activity of the enzyme. The biochemical evidence for such control and the results of numerical computations that show that the input–output behavior of the cells is accurately described by this model are given in these papers. We will refer to this model as the Monk-Othmer model. The model developed here is similar in spirit but quite different in detail. Recent experimental evidence discussed later demonstrates the involvement of G proteins in the signal transduction pathway and shows that calcium is involved in the PI cycle pathway. This opens the way for a more detailed analysis of the signal transduction process and, in particular, raises the possibility that the rapid component of relay adaptation arises in the transduction pathway without any direct involvement of calcium. In the present model the inhibition arises from a parallel inhibitory channel that provides a type of feedforward control, whereas in the Monk-Othmer model the primary control is via direct feedback.

Signal transduction via G proteins has been studied in a number of systems, including *Dd*, but is best characterized in mammalian systems. *Dd*-specific results are given in Section 2, and suffice it here to say that it is reasonable to assume that there are G_s, and G_i proteins present in the membrane. In other systems it is known that they couple the effects of stimulus and inhibitor. We base the model for the adenylate cyclase–activating pathway on what is known for mammalian cells, but, of course, in *Dd* the stimulus signal and inhibitory signal coincide. Since the single external cAMP has the dual effect of stimulation and inhibition, it is necessary, in order to get adaptation, to have two different receptors for external cAMP, and we call these R_s, and R_i. A novel feature of our model is that the inhibitory effect of G_i is at the receptor level. The activated G_i binds with the cAMP–R_s, complex and terminates its capacity for activating G_s. The detailed rationale behind the model is given in Section 2. In Section 3 we derive the equations that describe the model. Conservation conditions and singular perturbation techniques are used to reduce the numbers of differential equations involved. Some qualitative analysis of the model is done in Section 4 in order to develop an intuitive understanding of how this model functions.

Numerical results are presented in Section 5. The results show good agreement with experimental data from perfusion experiments. As was found in previous papers [32–37], this implies that the model should also reproduce the results for suspension experiments and for wave propagation in aggregation fields. The former is verified in Section 6, and results on the latter will be reported elsewhere. The results suggest that the fast component of adaptation can arise entirely within the adenylate cyclase–activating pathway; no coupling to other components such as the calcium or PI cycles is needed. This does not rule out the possibility that the PI cycle is involved in the adaptation process in *Dd*, and there is evidence for crosstalk between the cAMP pathway and the PI cycle pathway in *Dd* [23, 41]. Of course, theoretical analysis can never prove a model, and some experiments to test it are proposed in Section 7. The predicted outcomes of the proposed experiments are obtained via computer simulations. In the Appendix we give estimates for the parameters involved in the system. Some of the data needed are available from experiments on *Dd*, and some are estimated from other systems.

2. THE SIGNAL PATHWAYS FROM STIMULUS TO cAMP GENERATION

2.1. HORMONAL CONTROL OF ADENYLATE CYCLASE ACTIVITY IN MAMMALIAN CELLS

Recent research on the role of G proteins in the activation of adenylate cyclase has established some of the main steps in transmembrane signal transduction in numerous systems [21, 26, 30, 43–45]. In this section we give a brief review of the results known for the mammalian cAMP pathway in order to establish a basis for the mathematical model developed later.

While there are different membrane-bound receptors for different stimuli in this pathway, they fall into two classes that are generally denoted R_s and R_i. R_s is the receptor for agonist signals H_s, such as epinephrine, glucagon, and the β-adrenergic agonists. Antagonist signals H_i are transduced through the R_i receptor, examples of which include the α_2-adrenoceptor and the muscarinic M_2 receptor. R_i receptors may also respond to stimulus hormones [3, 14,47], which is the case in *Dd*. The R_s receptors are coupled to a single pool of a G protein denoted G_s, which is a heterotrimeric protein comprising an α_s subunit, a β subunit, and a γ subunit.

A typical scheme for signal transduction is shown in Figure 1. Upon binding of agonist to a receptor, the agonist–receptor complex H_sR_s catalyzes the conversion of G_s from the inactive GDP-binding state, to the active GTP-binding state, with the release of GDP and the $\beta\gamma$ subunits. Binding of the active G_s protein, which we denote by G_s' or α_sGTP, with the unactivated adenylate cyclase, which we denote UC, converts the latter into the activated cyclase AC. α_sGTP is deactivated by the intrinsic GTPase activity of α_s. Modulo the basal rate for the unactivated cyclase, the rate at which cAMP is produced is proportional to the amount of agonist present, and a constant level of stimulus can sustain a constant level of cAMP production in the absence of adaptation.

The reactions in the inhibitory pathway are not as well established. It is known that a specific protein G_i, which is the transducer of inhibitory signals, exists in the membrane. The mechanism for activating G_i is the same as that for activating G_s: H_iR_i catalyzes the exchange of GTP for GDP on G_i, which decomposes into $\beta\gamma$ and α_iGTP. G_i' (or α_iGTP), the active state of G_i, then turns off activation of adenylate cyclase by a mechanism that is not yet completely understood. G_i also has a three- subunit structure comprising α_i, β, and γ subunits. The β and γ subunits are identical to the β and γ subunits of G_s, but α_i is different from from α_s.

Many of the details of the transducing process are not known, even in the best-characterized systems. Some of these are discussed briefly in order to explain how we arrived at the model.

• Is G_s precoupled with adenylate cyclase? The issue here is whether H_sR_s interacts with the G_sUC complex, or whether H_sR_s interacts with G_s first, releasing G_s', after which G_s' reacts with UC. Levitzki [27] argues that G_s is always coupled to adenylate cyclase in vivo. This argument is based on the work of Arad et al. [2] and on kinetic analysis, which indicates that

the interaction between G_s and adenylate cyclase is not rate-limiting [27, 46]. Gilman [21] believes that this conclusion is not correct, based on the behavior in the presence of detergent and the excess of the amount of G_s over adenylate cyclase observed in vivo (cf. also [1] concerning the amounts of G_s and cyclase). Even though the experiments show that the rate is first-order in the hormone–receptor complex, one cannot conclude that G_s and UC are always bound; it may simply be that the rate of binding of G_s' to UC is large relative to other rates in the pathway, and this is what is assumed later in the model.

• Does G_i' interact directly with UC? In view of the fact that G_i and G_s have very similar structures, it is conceivable that G_i' interacts directly with adenylate cyclase, just as G_s' interacts with UC. If the inhibitory effect of G_i' is only competitive, then either there must be a large amount of G_i' present, or the binding of G_i' to UC must be very tight in order to turn off the signal. However, all attempts to identify a G_i'AC complex have failed [29]. Thus it is widely accepted that G_i' does not interact with UC directly to express the inhibitory effect.

• Does the subunit exchange hypothesis explain inhibition? Gilman proposed the “subunit exchange hypothesis” based on the observations that G_i is usually present at a higher concentration than G_s in vivo and that the subunits of β and γ in G_i and G_s are identical. He argued that the $\beta\gamma$ subunits released by G_i' will have a much higher concentration than G_s' and can reduce the amount of free G_s' by displacing the reaction equilibrium toward the inactive G_s form [7, 19, 44].

There are several difficulties with this hypothesis, as was noted by Levitzki [29]. First, he argues that his recent work suggests that the $\beta\gamma$ subunit plays no regulatory role. Second, if Gilman’s mechanism were operative, then the activation of any G protein with the same $\beta\gamma$ subunit would result in the inhibition of adenylate cyclase, even if it is not in the pathway in question. In the analysis given in the following section it will be seen that even though $\beta\gamma$ subunits may account for some inhibitory effect, it would not be enough to account for full adaptation in *Dd*.

• Does G_i or G_i' interact with H_sR_s? In [27] it is found that the β-adrenoceptor catalyzes the binding of GTPγS to G_i with an efficiency that is 30% of that for the activation of G_s. Levitzki remarks that “these interesting observations point to the possibility that G_i may mediate inhibition of adenylate cyclase not only directly on the catalytic subunit or via the $\beta\gamma$ subunits released from G_i and scavenging α_s, but also exerting its inhibitory effect on stimulatory receptors.” Thus, G_i does not have to carry out its inhibitory effect through the interaction with adenylate cyclase or G_s, but can do so through H_sR_s [28], which means that the effects of G_s and G_i are not symmetric. Levitzki suggests that in the absence of hormone, R_s, is bound with G_i, and that binding of hormone frees that receptor to catalyze the activation of G_s. However, in *Dd* the agonist and antagonist are identical, and it is difficult to see how the signal would be turned off. Later in this section we describe a scheme for *Dd* in which G_i' interacts directly with H_sR_s.

2.2. THE EVIDENCE FOR G PROTEIN-BASED TRANSDUCTION IN Dd

Several classes of cAMP receptors have been identified in *Dd*, and the dissociation constants for these receptors have been measured [49, 50]. Recently, significant progress has been made in understanding the signal pathway leading to the activation of adenylate cyclase. Gilman [21] set forth criteria for determining whether G proteins are involved in signal transduction, and van Haastert and coworkers [5, 40, 50] have concluded that the adenylate cyclase activation pathway in *Dd* meets several of these criteria. A G_α protein ($G_{\alpha 2}$) that may be involved in signal transduction has been identified, and since it does not have a site for ADP ribosylation catalyzed by pertussis toxin [18], it may be involved in the stimulatory channel.

In other systems pertussis toxin catalyzes the ADP ribosylation of α_iGDP, which blocks its inhibitory effect. If there is a G_i protein that modulates inhibition in *Dd*, then one expects that adaptation would be abolished when pertussis toxin is applied, and this is precisely what is observed experimentally [39–41]. In the experiment the initial increase of cAMP was identical in control and pertussis toxin–treated cells, which suggests that activation of adenylate cyclase is not affected, but cAMP synthesis continued in toxin-treated cells, due to a strongly diminished desensitization. This suggests that pertussis toxin plays the same role in *Dd* as it does in mammalian cells. G_s is not affected by pertussis toxin; hence the stimulatory pathway is not affected.

It is also known that cAMP induces phosphorylation of the cAMP receptors in *Dd* [24, 25] and that this occurs on the same time scale as adaptation. Thus phosphorylation may be involved in adaptation, perhaps by interfering with the activation of a G_s protein. However, phosphorylation is not sufficient for adaptation, since pertussis toxin treatment blocks adaptation but does not interfere with receptor modification [40, 50]. This suggests that activation of a G_i protein is necessary for adaptation [42]. In our model we propose one scheme by which this might occur and show that it can produce the observed adaptation. To simplify the scheme we do not include a role for phosphorylation, but in the conclusion section we indicate how this can be incorporated and what effects this would have on the dynamics. This leaves us with three possible patterns of interactions for adaptation: (i) G_i' can interact with adenylate cyclase directly; (ii) G_i' may possibly turn off the signal by buffering G_s' via the $\beta\gamma$ subunits; and (iii) G_i' can interact with cAMP–R_s directly.

(i) If the G protein network is as in other systems, then it is unlikely that G_i' interacts with adenylate cyclase directly, and the scheme shown in Figure 2, which was suggested in [39]–[41], is questionable. However, such a scheme is not unworkable, for if we suppose that G_i' interacts with G_s'AC to turn off the enzyme, then numerical simulations indicate that the experimental results can be reproduced. This point will be elaborated in the conclusion section.

(ii) The ratio of G_s to G_i is very important here. If the concentration of G_i is much greater than that of G_s, then it is possible that the $\beta\gamma$ subunits released from G_i can buffer G_s', and complete adaptation can result. However, if the concentration of G_s is greater than about

10% of G_i, there will be a significant amount of free G_s' and thus a significant steady-state rate of cAMP production, which is at variance with observations for *Dd*. Moreover, the concentrations of G_s and G_i proteins are approximately the same in *Dd* under the assumption that they are proportional to the concentrations of the corresponding receptors [49].

(iii) A model based on the interaction of G_i' with cAMP–R_s can explain the adaptation process and other experimental results. As we remarked earlier, it is difficult to obtain adaptation if G_i interacts directly with cAMP–R_s. Thus we propose the following scheme.

$$\begin{aligned} G_i' + H_sR_s &\rightarrow H_sR_sG_i' \\ H_sR_sG_i' &\rightarrow H_s + R_s + G_i' \\ H_sR_sG_i' &\rightarrow H_sR_s + \alpha_i \mathrm{GDP} \end{aligned} \qquad (1)$$

This mechanism is supported by several facts.

• It is found in other systems that an increase in the GTP concentration causes a decrease in the concentration of the H_sR_s complex but has little effect on the H_iR_i complex [27, 31]. In our mechanism the decrease in $[H_sR_s]$ due to the increase in [GTP] is mediated through the increase in $[G_i']$. The formation of $H_sR_sG_i'$ and its rapid decomposition leads to a decrease in the concentration of the H_sR_s complex.

• The affinity of R_s for H_s is decreased in the presence of G_i' [31, 49]. In the proposed scheme this results from the rapid decomposition of the $H_sR_sG_i'$ complex.

The detailed mechanism for relay adaptation, of which the above is one component, is described in the next section.

3. THE MATHEMATICAL MODEL

The reactions in the mechanism are as follows. Here and hereafter we use H to represent the extracellular cAMP stimulus.

(i) The Stimulus Pathway

$$H + R_s \underset{k_{-1}}{\overset{k_1}{\rightleftharpoons}} HR_s \qquad (2a)$$

$$HR_s + G_s \underset{k_{-2}}{\overset{k_2}{\rightleftharpoons}} HR_sG_s \qquad (2b)$$

$$HR_sG_s + GTP \xrightarrow{\hat{k}_3} HR_s + G'_s + GDP + \beta\gamma \quad (2c)$$

$$G'_s + UC \underset{k_{-4}}{\overset{k_4}{\rightleftharpoons}} G'_sAC \quad (2d)$$

$$G'_s \xrightarrow{k_s} \alpha_s GDP + P_i \quad (2e)$$

$$G'_sAC \xrightarrow{k_s} \alpha_s GDP + UC + P_i \quad (2f)$$

$$\alpha_s GDP + \beta\gamma \xrightarrow{k_6} G_s \quad (2g)$$

(ii) The Inhibitory Pathway

$$H + R_i \underset{h_{-1}}{\overset{h_1}{\rightleftharpoons}} HR_i \quad (3a)$$

$$HR_i + G_i \underset{h_{-2}}{\overset{h_2}{\rightleftharpoons}} HR_iG_i \quad (3b)$$

$$HR_iG_i + GTP \xrightarrow{\hat{h}_3} HR_i + G'_i + GDP + \beta\gamma \quad (3c)$$

$$G'_i + HR_s \underset{h_{-4}}{\overset{h_4}{\rightleftharpoons}} HR_sG'_i \quad (3d)$$

$$G_i' \xrightarrow{h_5} \alpha_i GDP + P_i \quad (3e)$$

$$HR_sG_i' \xrightarrow{h_6} H + R_s + G_i' \quad (3f)$$

$$HR_sG_i' \xrightarrow{h_5} HR_s + \alpha_i GDP + P_i \quad (3g)$$

$$\alpha_i GDP + \beta\gamma \xrightarrow{h_7} G_i \quad (3h)$$

(iii) Production and Secretion of Intracellular cAMP

$$G_s'AC + ATP \underset{\hat{l}_{-1}}{\overset{\hat{l}_1}{\rightleftharpoons}} G_s'AC - ATP \quad (4a)$$

$$G_s'AC - ATP \xrightarrow{l_2} cAMP_i + G_s'AC \quad (4b)$$

$$cAMP_i + iPDE \underset{l_{-3}}{\overset{l_3}{\rightleftharpoons}} cAMP_i - iPDE \quad (4c)$$

$$cAMP_i - iPDE \xrightarrow{l_4} AMP + iPDE \quad (4d)$$

$$cAMP_i \xrightarrow{l_5} cAMP_o^* \quad (4e)$$

The definition of the symbols used in these reactions is given in Table 1, as are the mathematical symbols used later. The function l_5 is the secretion rate function, and we assume here that it is linear. In the perfusion experiments, the secreted cAMP must be

distinguished from cAMP in the perfusate, since the former is radioactively labeled. We use an asterisk (*) to indicate the former.

The basic assumptions concerning the transduction component of the model are the following.

• The G_s and G_i proteins exist unbound in the membrane and act as shuttle messengers in the presence of cAMP. In the inactive GDP-bound form, the α subunit of each has a high affinity for the $\beta\gamma$ subunit.

• The $\beta\gamma$ subunit is released upon the activation of the G protein. The $\beta\gamma$ subunits of G_s and G_i are identical.

• The roles of G_s and G_i are not symmetric. G_s' combines with inactive adenylate cyclase and transforms it to its active form, while G_i' combines with the activated form of R_s, cAMP–R_s, and converts it to its inactive form R_s by releasing cAMP.

• The hydrolyzation rates of G_x', where x = s or i, are the same for all states, that is, for G_s, G_s', G_s'AC, G_s'AC – ATP and for G_i, G_i', cAMP–$R_s G_i'$. (This assumption is not essential and can be easily changed. In reality, G_s'AC, G_s'AC – ATP, and cAMP–$R_s G_i'$ may have a higher rate of hydrolysis than G_s' and G_i').

There are three interacting pathways involved: (1) the stimulus pathway, which involves signal transduction from extracellular cAMP to R_s, from R_s to G_s, and from G_s to adenylate cyclase; (2) the inhibitory pathway, in which the extracellular signal is transduced into an inhibitory intracellular signal; and (3) the pathway for the generation and secretion of intracellular cAMP. If extracellular cAMP is a dynamic variable, as in the suspension experiments, the stimulus, production, and secretion pathways form a positive feedback loop. This loop is controlled by negative feedback from the parallel inhibitory pathway, as shown in Figure 3. Clearly the dynamics will depend strongly on the characteristic time scales of the positive and negative feedback loops. When viewed at the level of cAMP production, which is the output, these parallel pathways constitute a feedforward control loop in which the disturbance signal is measured, processed, and used to turn off cAMP production and secretion (see Figure 3). The preset value for the system is the basal cAMP turnover rate of UC. The external disturbance is the increase in the extracellular cAMP concentration. This increase is detected by the “observer” R_i and by the “processor,” which is the inhibitory pathway. The feedforward signal acts at R_s, and in this way the “disturbance” is greatly reduced before it enters the “system,” which comprises G_s and UC.

Certain of the species involved in the model are assumed to be constant, and their effects are included in the kinetic constants. These are GTP, GDP, ATP, P_i, AMP, and other species that may influence the reactions. Furthermore, in the “mechanism” given below, we neglect unimportant back-reactions and reactions that generate short-lived intermediates such as $HR_s\alpha_s GTP\beta\gamma$ and $R_s G_i'$. Furthermore, we neglect the hydrolysis of activated adenylate cyclase bound with substrate, and we neglect the basal (unactivated) activity of the cyclase.

Notice that the nature of the reactions between G_i' and the cAMP–R_s complex is different than that of the reactions between G_s' and UC. The effect of G_s' is to increase the binding rate between ATP and adenylate cyclase by activating adenylate cyclase, while the effect of G_i' is to decrease the rate of the binding between extracellular cAMP and R_s by deactivating R_s. The rapid decomposition of cAMP$-R_sG_i'$ accounts for the apparent loss of affinity of R_s for extracellular cAMP. Of course, once the complex decomposes, extracellular cAMP can bind to the bare receptor again. An increase in the GTP concentration will cause an increase of G_i', which in turn causes a loss of affinity of R_s to extracellular cAMP and a decrease in the total amount of cMAI–R_s complex in the steady state.

For simplicity, we only display the differential equations for the variables y_1–y_{14}, since the remaining unknowns can be obtained from conservation conditions. There are seven conservation relations for the system, and the quantities that are determined by these relations are listed in Table 2. The differential equations for quantities in the stimulus pathway are

$$\begin{aligned}
\frac{dy_1}{dt} &= k_1 H z_1 - k_{-1} y_1 - k_2 y_1 z_2 + (k_{-2} + k_3) y_2 - h_4 y_1 y_8 + h_5 y_9, \qquad (5)\\
\frac{dy_2}{dt} &= k_2 y_1 z_2 - (k_{-2} + k_3) y_2,\\
\frac{dy_3}{dt} &= k_3 y_2 - k_4 y_3 z_3 - k_5 y_3,\\
\frac{dy_4}{dt} &= k_4 y_3 z_3 - (k_5 + l_1) y_4 + (l_{-1} + l_2) y_{11},\\
\frac{dy_5}{dt} &= k_5 (y_3 + y_4) - k_6 y_5 z_6 .
\end{aligned}$$

The differential equations for quantities in the inhibitory pathway are

$$\begin{aligned}
\frac{dy_6}{dt} &= h_1 H z_4 - h_{-1} y_6 - h_2 y_6 z_5 + (h_{-2} + h_3) y_7, \qquad (6)\\
\frac{dy_7}{dt} &= h_2 y_6 z_5 - (h_{-2} + h_3) y_7\\
\frac{dy_8}{dt} &= h_3 y_7 - h_4 y_1 y_8 - h_5 y_8 + h_6 y_9,\\
\frac{dy_9}{dt} &= -(h_5 + h_6) y_9 + h_4 y_1 y_8,\\
\frac{dy_{10}}{dt} &= h_5 (y_8 + y_9) - h_7 y_{10} z_6 .
\end{aligned}$$

The differential equations for the production and secretion of intracellular cAMP are

$$\begin{aligned}
\frac{dy_{11}}{dt} &= l_1 y_4 - (l_{-1} + l_2) y_{11}, \qquad (7)\\
\frac{dy_{12}}{dt} &= l_2 y_{11} - l_5 y_{12} + l_{-3} y_{13} - l_3 y_{12} z_7,\\
\frac{dy_{13}}{dt} &= -(l_{-3} + l_4) y_{13} + l_3 y_{12} z_7,\\
\frac{dy_{14}^*}{dt} &= l_5 y_{12}.
\end{aligned}$$

Here $k_3 \equiv \hat{k}_3[\mathrm{GTP}]$, $h_3 \equiv \hat{h}_3[\mathrm{GTP}]$, and $l_1 \equiv \hat{l}_1[\mathrm{ATP}]$.

The conservation relations that determine the dependent variables z_i, $i = 1, \ldots, 7$, are

$$\begin{aligned}
&y_1 + y_2 + y_9 + z_1 = [\mathrm{R_s}]_T, \qquad (8)\\
&y_2 + y_3 + y_4 + y_5 + y_{11} + z_2 = [\mathrm{G_s}]_T,\\
&y_4 + y_{11} + z_3 = [\mathrm{UC}]_T, \quad y_6 + y_7 + z_4 = [\mathrm{R_i}]_T,\\
&y_7 + y_8 + y_9 + y_{10} + z_5 = [\mathrm{G_i}]_T,\\
&y_3 + y_4 + y_5 + y_8 + y_9 + y_{10} + y_{11} - z_6 = 0,\\
&y_{13} + z_7 = [\mathrm{iPDE}]_T,
\end{aligned}$$

where subscript T denotes the initial value of a quantity. When these are solved for the z_i and the solutions used in (5)–(7), the result is a system of 13 equations in $y_1, \ldots, y_{13}$, with at worst quadratic nonlinearities. The reader can easily show that the flow associated with these equations preserves positivity, that is, solutions of these equations that begin in the nonnegative cone of composition space remain there. Furthermore, it is easy to see that $y_1, \ldots, y_{11}$ and y_{13} remain bounded for all time, and the bounds are given in Table 3. If appropriate assumptions are made about the secretion function and the rate constants for adenylate cyclase and intracellular phosphodiesterase, then the same is true of y_{12}. Thus the governing equations are well-posed in the mathematical sense.

4. ANALYSIS OF THE MODEL

In this section we describe the qualitative behavior of the model, we do a reduction that simplifies the system, and we analyze various components of the dynamics.

4.1. A QUALITATIVE DESCRIPTION OF ADAPTATION AND DEADAPTATION IN THE MODEL

Suppose that a step change in the extracellular concentration of cAMP is introduced in a perfusion apparatus. Since agonist and antagonist are the same in *Dd*, $\mathrm{G_i'}$ and $\mathrm{G_s'}$ will be produced simultaneously. $\mathrm{G_s'}$ activates UC, while $\mathrm{G_i'}$ combines with $\mathrm{HR_s}$ to deactivate it. This blocks the further production of $\mathrm{G_s'}$, and the $\mathrm{G_s'}$ produced in response to the step will be degraded by hydrolysis. Thus there will be an initial burst of cAMP produced, but the

activated adenylate cyclase will decay due to the hydrolysis of G'_s. If a higher concentration is presented, then a new burst of G'_s and G'_i will be produced. As we shall see, if the time scales in the stimulatory and inhibitory channels are adjusted properly, this mechanism can produce the full range of observations in perfusion and suspension experiments. The qualitative time course of the various species following a step change in cAMP is shown in Figure 4. In [39], cAMP secretion was compared in pertussis-treated and untreated cells, and it was found that for the first 30 s of stimulus the secretion rates were the same. This indicates that the lag time in the inhibitory pathway, which is $T_{l1} + T_{l2}$ in Figure 4, is of the order of 30 s.

If a constant cAMP stimulus that has been held long enough to produce full adaptation is terminated, the concentration of the HR_s and HR_i complexes will decay. Decay of HR_i, produces no new G'_i, and the amount of $HR_sG'_i$ will decrease due to hydrolysis. Under the assumption that hydrolysis is first-order in the substrate, deadaptation occurs at an exponential rate when the stimulus is withdrawn.

4.2. NONDIMENSIONALIZATION AND REDUCTION OF THE EQUATIONS

Nondimensionalization.—We start by introducing dimensionless variables for the 14 independent concentration variables. The choices of dimensionless variables depend on the estimates of kinetic parameters, which are derived in the Appendix. The results are summarized in Tables 4 and 5.

After nondimensionalization, one finds that the dimensionless variables fall into two categories: those that reach a pseudo-steady state rapidly, which we call the singular variables, and the remainder, which we call nonsingular variables. The mathematical symbols for singular variables are v_i, $i = 1, \ldots,6$, and for nonsingular variables u_i, $i = 1, \ldots,8$. The dimensionless variables and their relationship to the corresponding dimensional variables are listed in Table 6. The nondimensionalization gives rise to a number of small parameters, which are defined in Table 7. Other dimensionless kinetic parameters are listed in Table 8. Note that $\tau \sim \mathcal{O}(1)$ corresponds to $t \sim \mathcal{O}(10\ \mathrm{s})$.

The dimensionless form of (5)–(7), wherein the conservation equations have been used to remove z_i, is as follows. The differential equations for the singular variables are

$$\epsilon_1\frac{dv_1}{d\tau} = u_1 - v_1 - u_1\left(u_2 + u_3 + \epsilon_1 c_1\alpha_2 v_1 + \epsilon_2 v_2 + \epsilon_5 c_1\gamma_1 v_5\right),$$
$$\epsilon_2\frac{dv_2}{d\tau} = u_2 + u_3 - v_2\left(u_2 + u_3 + \frac{c_1}{c_3}u_5 + c_1 u_6 + \epsilon_2 v_2 + \epsilon_4\frac{c_1}{c_3}\beta_5 v_4 + \epsilon_5\gamma_1 v_5\right),$$
$$\epsilon_3\frac{dv_3}{d\tau} = u_4 - v_3 - u_4\left(u_5 + c_3 u_6 + \epsilon_3\beta_2 v_3 + \epsilon_4 c_2\beta_5 v_4\right),$$
$$\epsilon_4\frac{dv_4}{d\tau} = u_5 + c_3 u_6 - \frac{c_3}{c_1}v_4\left(u_2 + u_3 + \frac{c_1}{c_3}u_5 + c_1 u_6 + \epsilon_2 v_2 + \epsilon_4\frac{c_1}{c_3}\beta_5 v_4 + \epsilon_5\gamma_1 v_5\right),$$
$$\epsilon_5\frac{dv_5}{d\tau} = u_3 - v_5,$$
$$\epsilon_6\frac{dv_6}{d\tau} = u_7 - v_6 - \frac{1}{\gamma_3}u_7 v_6, \tag{9}$$

and the differential equations for the nonsingular variables are

$$\frac{du_1}{d\tau} = \alpha_H(\tau) - \left[\alpha_H(\tau) + \alpha_1 + \alpha_2\right]u_1 + \left[1 - \epsilon_1\alpha_H(\tau)\right]\alpha_2 v_1 + \left[\beta_5 - \alpha_H(\tau)\right]u_6 - \beta_4 u_1 u_5$$
$$+ \alpha_2 u_1\left(u_2 + u_3 + \epsilon_1 c_1\alpha_2 v_1\epsilon_2 v_2 + \epsilon_5\gamma_1 v_5\right),$$
$$\frac{du_2}{d\tau} = \alpha_2\alpha_3 c_1 v_1 - \left(1 + \alpha_4\right)u_2 + \alpha_4 u_2\left(u_3 + \epsilon_5\gamma_1 v_5\right),$$
$$\frac{du_3}{d\tau} = \alpha_4 u_2 - \left(1 + \gamma_1\right)u_3 + \gamma_1 v_5 - \alpha_4 u_2\left(u_3 + \epsilon_5\gamma_1 v_5\right),$$
$$\frac{du_4}{d\tau} = \beta_H(\tau) - \left[\beta_H(\tau) + \beta_1 + \beta_2\right]u_4 + \left[1 - \epsilon_3\beta_H(\tau)\right]\beta_2 v_3$$
$$+ \beta_2 u_4\left(u_5 + c_3 u_6 + \epsilon_3\beta_2 v_3 + \epsilon_4\beta_5 v_4\right),$$
$$\frac{du_5}{d\tau} = -\beta_5 u_5 + \beta_6 c_3 u_6 + \beta_2\beta_3 c_2 v_3 - c_3\beta_4 u_1 u_5,$$
$$\frac{du_6}{d\tau} = -\left(\beta_5 + \beta_6\right)u_6 + \beta_4 u_1 u_5,$$
$$\frac{du_7}{d\tau} = \gamma_1\gamma_2 v_5 - \gamma_5 u_7 - \frac{l_3[\mathrm{iPDE}]_T}{k_5}u_7 + \frac{l_{-3}}{k_5\gamma_3}v_6 + \frac{l_3[\mathrm{iPDE}]_T}{k_5\gamma_3}u_7 v_6,$$
$$\frac{du_s^*}{d\tau} = \gamma_5 u_7\,. \tag{10}$$

Upper and lower bounds for the solution in dimensionless terms are given in Table 9. In deriving these it is assumed that the initial conditions satisfy the conservation equations and lie inside the bounded region.

Simplification via Singular Perturbation.—On the τ time scale, the singular equations can be reduced to the algebraic system

$$
\begin{aligned}
&u_1 - v_1 - u_1\left(u_2 + u_3 + \epsilon_1 c_1 \alpha_2 v_1 + \epsilon_2 v_2 + \epsilon_5 c_1 \gamma_1 v_5\right) = 0, \\
&u_2 + u_3 - v_2\left(u_2 + u_3 + \frac{c_1}{c_3}u_5 + c_1 u_6 + \epsilon_2 v_2 + \epsilon_4 \frac{c_1}{c_3}\beta_5 v_4 + \epsilon_5 \gamma_1 v_5\right) = 0, \\
&u_4 - v_3 - u_4\left(u_5 + c_3 u_6 + \epsilon_3 \beta_2 \nu_3 + \epsilon_4 c_2 \beta_5 v_4\right) = 0, \\
&u_5 + c_3 u_6 - \frac{c_3}{c_1}v_4\left(u_2 + u_3 + \frac{c_1}{c_3}u_5 + c_1 u_6 + \epsilon_2 v_2 + \epsilon_4 \frac{c_1}{c_3}\beta_5 v_4 + \epsilon_5 \gamma_1 v_5\right) = 0, \\
&y_3 - v_5 = 0, \\
&u_7 - v_6 - \left(1/\gamma_3\right)u_7 v_6 = 0.
\end{aligned}
\tag{11}
$$

The solution of this system to within terms of $\mathcal{O}(\epsilon_i)$ is

$$
\begin{aligned}
v_1 &= u_1 - u_1\left(u_2 + u_3\right), \\
v_2 &= \frac{u_2 + u_3}{u_2 + u_3 + \left(c_1/c_3\right)u_5 + c_1 u_6}, \\
v_3 &= u_4 - u_4\left(u_5 + c_3 u_6\right), \\
v_4 &= \frac{c_1\left(u_5 + c_3 u_6\right)}{c_3\left[u_2 + u_3 + \left(c_1/c_3\right)u_5 + c_1 u_6\right]}, \\
v_5 &= u_3, \\
v_6 &= \gamma_3 u_7/\left(u_7 + \gamma_3\right).
\end{aligned}
\tag{12}
$$

If we replace the v_i in Equation (10) by their pseudo-steady-state values given by Equation (12), then we get an ordinary differential equation system with seven independent variables. We can also approximate this differential equation system by dropping the $\mathcal{O}(\epsilon)$ and higher order terms, where $\epsilon \equiv \max\{\epsilon_i\}$. After some simplifications, we obtain the following system.

$$\frac{du_1}{d\tau} = \alpha_H(\tau) - \left[\alpha_H(\tau) + \alpha_1\right]u_1 + \left[\beta_5 - \alpha_H(\tau)\right]u_6 - \beta_4 u_1 u_5, \tag{13}$$

$$\frac{du_2}{d\tau} = \alpha_2\alpha_3 c_1 u_1 - \left(1 + \alpha_4\right)u_2 - \alpha_2\alpha_3 c_1 u_1\left(u_2 + u_3\right) + \alpha_4 u_2 u_3,$$

$$\frac{du_3}{d\tau} = \alpha_4 u_2 - u_3 - \alpha_4 u_2 u_3,$$

$$\frac{du_4}{d\tau} = \beta_H(\tau) - \left[\beta_H(\tau) + \beta_1\right]u_4,$$

$$\frac{du_5}{d\tau} = \beta_2\beta_3 c_2 u_4 - \beta_5 u_5 + \beta_6 c_3 u_6 - c_3\beta_4 u_1 u_5 - \beta_2\beta_3 c_2 u_4\left(u_5 + c_3 u_6\right),$$

$$\frac{du_6}{d\tau} = -\left(\beta_5 + \beta_6\right)u_6 + \beta_4 u_1 u_5,$$

$$\frac{du_7}{d\tau} = \gamma_1\gamma_2 u_3 - \gamma_5 u_7 - \frac{\gamma_4 u_7}{u_7 + \gamma_3},$$

$$\frac{du_8^*}{d\tau} = \gamma_5 u_7 .$$

4.3. ANALYSIS OF THE COMPONENT STEPS

We next analyze the qualitative dynamics of the model. For convenience in relating the results to the biochemical steps, we do this in terms of the dimensional quantities. First we analyze various individual steps by uncoupling the pathways. The second part is devoted to the study of the coupled system. In this case the dynamics cannot be analyzed directly, but with certain simplifications we can analyze the steady-state behavior. This provides some qualitative understanding of how adaptation arises.

The Dynamics of G-Protein Activation.—We first suppose that $k_4 = h_4 = 0$, which suppresses activation of AC and inactivation of HR_s. This enables us to uncouple the three pathways and study the dynamics of G-protein activation.

First consider the binding to R_s, for which the reactions are (2a) and (2b). We invoke the pseudo-steady-state assumption for $[HR_sG_s]$ to reduce the degrees of freedom, by setting

$$\frac{d\left[\mathrm{HR_sG_s}\right]}{dt} = 0.$$

In this way, we obtain the usual expression

$$\left[\mathrm{HR_sG_s}\right] = \frac{k_2}{k_{-2} + k_3}\left[\mathrm{HR_s}\right]\left[\mathrm{G_s}\right],$$

and according to our estimates of parameters,

$$\frac{[HR_sG_s]}{[R_s]_T} = \frac{k_2[R_s]_T}{k_3}\left(\frac{[G_s]}{[R_s]_T}\right)\left(\frac{[HR_s]}{[R_s]_T}\right) \leqslant 1.67\times 10^{-4}\frac{[HR_s]}{[R_s]_T}.$$

Hence the amount of HR_sG_s is very small compared to $[HR_S]$, and therefore we have the approximation

$$\frac{d[HR_s]}{dt} = k_1[H][R_s] - k_{-1}[HR_s],$$

$$[HR_s] + [R_s] = [R_s]_T$$

or equivalently,

$$\frac{dy_1}{dt} = k_1[H][R_s]_T - (k_1[H] + k_{-1})y_1, \quad y_1(0) = 0. \quad (14)$$

Thus the response is

$$y_1(t) = [R_s]_T\frac{[H]}{[H] + K_d}\left(1 - e^{-(k_1[H] + k_{-1})t}\right), \quad (15)$$

where $K_d \equiv k_{-1}/k_1$ is the dissociation constant. This process is fast because k_{-1} is relatively large. The half-time for this process is

$$t^{0.5} = \frac{\ln 2}{k_1[H] + k_{-1}} < \frac{\ln 2}{k_{-1}} = 1.54 \text{ s},$$

and the steady-state response is

$$u_1^d \equiv \frac{[HR_s]_s}{[R_s]_T} = \frac{[H]}{[H] + K_d}, \quad (16)$$

where $[\cdot]_s$ denotes the steady-state concentration of a species. A similar analysis can be done for the binding of cAMP to R_i.

Next we consider the activation of G_s by HR_s. The reactions involved are (2b), (2c), (2e), and (2g). Our estimates of the parameters (cf. Appendix) shows that k_6 is very large. Hence $[\alpha_s GDP]$ is small, and we simplify the analysis by setting $[\alpha_s GDP] = 0$. The simplified reaction and conservation equations are

$$\frac{d[G'_s]}{dt} = k_3[HR_sG_s] - k_5[G'_s],$$

$$[HR_sG_s] = \frac{k_2}{k_{-2}+k_3}[HR_s][G_s],$$

$$[G_s]_T = [G_s] + [G'_s] + [HR_sG_s],$$

and therefore

$$\frac{dy_3(t)}{dt} = k_{on}[G_s]_T - (k_{on}+k_s)y_3, \quad y_3(0) = 0, \quad (17)$$

where $k_{on} = k_2k_3/(k_{-2} + k_3)[HR_s]$. Here k_{on} is not a constant but is time-dependent. When the stimulus level is higher than 0.1 μM, the binding step is much faster than the activation of G'_s. Hence we can suppose that the binding is in equilibrium and use the value of $[HR_s]$ given by (16) in k_{on}. Consequently,

$$y_3(t) = \frac{k_{on}[G_s]_T}{k_{on}+k_5}\left(1 - e^{-(k_{on}+k_5)t}\right). \quad (18)$$

When [H] is smaller than 0.1 μM, the speed of the binding step is comparable to that of activation of G_s. In this case we cannot get an explicit solution, but in any case, the half-time for this response is estimated by

$$t^{0.5} = (\ln 2)/(k_{on}+k_5).$$

Using the estimate of k_{on} and k_{off}, we find that

$$3.0\text{ s} < t^{0.5} < 11.1\text{ s}.$$

Thus the steady-state response is given by

$$\frac{[G'_s]_s}{[G_s]_T} = \frac{k_{on}}{k_{on}+k_5} = \frac{k_2k_3[HR_s]_s}{k_2k_3[HR_s]_s + (k_{-2}+k_3)k_5}. \quad (19)$$

A similar analysis can be done for the activation of G_i. The biochemical reactions involved are (3b), (3c), (3e), and (3h), since $HR_sG'_i = 0$. Because h_7 is large, we neglect $[\alpha_i GDP]$ and obtain the approximate solution

$$y_8(t) = \frac{h_{\text{on}}[\text{G}_i]_T}{h_{\text{on}} + h_5}\left(1 - e^{-(h_{\text{on}} + h_5)t}\right), \quad (20)$$

where $h_{\text{on}} = [h_2 h_3/(h_{-2} + h_3)][\text{HR}_\text{i}]$. The half-time for this response is

$$t^{0.5} = (\ln 2)/(h_{\text{on}} + h_5),$$

and using our estimates of h_{on} and h_{off} we obtain

$$39.6 \text{ s} < t^{0.5} < 92.4 \text{ s}.$$

Thus in the absence of coupling, the delay in the buildup of $[\text{G}_\text{i}']$ is of the same order as the observed adaptation time.

The steady-state response is given by

$$\frac{[\text{G}_\text{i}']_s}{[\text{G}_\text{i}]_T} = \frac{h_{\text{on}}}{h_{\text{on}} + h_5} = \frac{h_2 h_3 [\text{HR}_\text{i}]_\text{s}}{h_2 h_3 [\text{HR}_\text{i}]_\text{s} + (h_{-2} + h_3) h_5}.$$

Table 10 shows the steady-state response of receptor binding and activation of the G proteins for different stimulus levels, using the parameter values estimated in the Appendix. From this table one sees how the fractions of the activated G proteins depend on the stimulus level.

A Steady-State Analysis of the Coupled System.—In this section, we will do the steady-state analysis for the coupled pathways, that is, for the case of $k_4 \neq 0$ and $h_4 \neq 0$. The three pathways are coupled, and we cannot obtain an explicit solution, but we can obtain some quantitative insight into adaptation.

The binding of external stimulus H with R_i is the same as in the case for the decoupled system, but $[\text{G}_\text{i}']$ will be different, since a fraction of the G_i' will be bound to HR_s. Since we assume that G_i' decays at the same rate irrespective of what form it is in, we may consider the combined concentration of the two forms of G_i', namely, G_i' and $\text{HR}_\text{s}\text{G}_\text{i}'$.

Let $[\text{G}_\text{i}'[*$ denote this quantity:

$$[\text{G}_\text{i}']^* = [\text{G}_\text{i}'] + [\text{HR}_\text{s}\text{G}_\text{i}']. \quad (21)$$

Reactions (3d) and (3g) do not alter $[\text{G}_\text{i}']^*$, and therefore it is dynamically equivalent to $[\text{G}_\text{i}']$ in the preceding analysis. As a result,

$$[G_i']^* = \frac{h_{on}[G_i]_T}{h_{on}+h_5}\left(1 - e^{-(h_{on}+h_s)t}\right). \quad (22)$$

Now consider the equations for $[HR_s]$ and $[HR_sG_i']$. The differential equations are

$$\frac{dy_1}{dt} = k_1[H]\left([R_s]_T - y_1 - y_9\right) - k_{-1}y_1 - h_4 y_1\left([G_i']^* - y_9\right), \quad (23)$$
$$\frac{dy_9}{dt} = k_4\left([G_i']^* - y_9\right)y_1 - h_6 y_9,$$
$$y_1(0) = y_9(0) = 0.$$

This system is closed since $[G_i']^*$ is given by (22), but we cannot find an explicit solution to it. Therefore we only do the steady-state analysis in order to obtain some insight as to how adaptation works in this step. With some simplifications we obtain the system

$$u_1^d - u_1 - \frac{k_1[H]+h_6}{k_1[H]+k_{-1}}u_6 = 0, \quad (24)$$
$$u_1 - \frac{[R_s]_T}{[G_i']_s^*}u_1u_6 - \frac{h_6}{h_4[G_i']_s^*}u_6 = 0,$$

where u_1^d is given in (16). The approximate solution is

$$u_1 = \left\{\frac{h_6}{h_6 + h_4[G_i]_s^*\left(k_1[H]+h_6\right)/\left(k_1[H]+k_{-1}\right)}\right\}u_1^d, \quad (25)$$

and since $u_1 = [HR_s]/[R_s]_T$, this represents the unadapted portion of $[HR_s]$. From this equation one can deduce the following:

- An increase in h_4 causes a decrease in $[HR_s]_s$, by virtue of reaction (3d).
- An increase in $[G_i']_s^*$ causes a decrease in $[HR_s]_s$. This can occur, for example, by increasing h_{on} or $[G_i]_T$.
- An increase in h_6 leads to an increase in $[HR_s]_s$, because HR_sG_i' decomposes faster.

One of the basic assumptions given in Section 3 is that the G_s' is hydrolyzed at the same rate irrespective of whether it is in free or bound form. An argument similar to that used to obtain $[G_i']^*$ shows that the combined concentrations of G_s', $G_s'AC$, and $G_s'AC - ATP$, which we

denote $[G'_s]^*_s$, is the same as the concentration of G'_s in the uncoupled system. Since $[HR_s]$ is very small at steady state (see Table 11), it follows from (19) that $[G'_s]_s$ and $[G'_sAC]_s$, are small. The last row of Table 11 gives the values of $[G'_s]^*_s$ corresponding to the parameters given in the Appendix. Thus we see that adaptation of internal cAMP production and secretion results from adaptation at the level of the stimulatory receptor.

5. NUMERICAL RESULTS

5.1. THE DYNAMICS OF THE UNCOUPLED SYSTEM

In the first set of simulations we let $k_4 = h_4 = 0$, with other parameters held at the values estimated in the Appendix. Typical response curves are shown in Figure 5 for a single-step stimulus. One can see that the response of both HR_s and HR_i is rapid; both reach their steady-state value within seconds. On the other hand, $[G'_s]$ and $[G'_i]$ increase on a much slower time scale, with the former increasing more rapidly and to a higher level than the latter.

If the steady-state response for a certain level of stimulus is independent of the stimulus history, then we say that the system exhibits steady-state additivity. This property is illustrated in Figure 6, where we show the response to a sequence of lo-fold increases in the stimulus. Comparison of Figures 5 and 6 shows that the steady-state response to a single step to $H = 0.1\ \mu M$ is the same as the response to a multistep stimulus ending at the same level, but the time-dependent portions of the responses are completely different.

The numerical responses for $[HR_s]$, $[HR_i]$, $[G'_s]$, and $[G'_i]$ are consistent with the results obtained from the qualitative analysis, which justifies the approximations we made in the previous section. We shall see later that $[HR_s]$ changes significantly in the coupled system compared to the uncoupled system, while $[HR_i]$ and $[G'_i]^*$, which is the combined amount of $[HR_sG'_i]$ and $[G'_i]$, change very little.

5.2. THE DYNAMICS OF THE COUPLED SYSTEM: EXPERIMENTAL AND NUMERICAL

The perfusion experiments done by Devreotes and coworkers [10, 13] provide a benchmark against which an adaptation model can be tested. The result of a typical experiment is shown in Figure 7. Note that the secretion rate does not adapt perfectly in this experiment.

The predicted cAMP secretion rate in response to the same stimulus is shown in Figure 8, where it is seen that the model also predicts incomplete adaptation. Note also that the predicted secretion rate peaks more rapidly for the estimated parameters than does the observed rate. The time to peak could be increased by decreasing either k_1 or k_4

The rapid buildup and decrease of $[HR_s]$ shown in Figure 8a illustrates the fact that adaptation to a constant stimulus occurs at the receptor level. Since the time scale of $[HR_s]$ is fast compared to the activation of G_s and adenylate cyclase, one can regard the signal carried by $[HR_s]$ as a δ function with a certain magnitude that depends on the stimulus levels. That is, the interaction of the stimulatory and inhibitory pathways generates a signal like a δ

function. If the signal transduction from G_s to adenylate cyclase can be approximately treated as a linear amplification process, then the response to this δ-function input would give the transient response of this process in a control-theoretic sense. However, the biochemical processes involved are not linear, but one should note that the response still has the shape of a first-order transient function.

As the stimulus level increases, the maximum secretion rate increases as well as the steady-state unadapted portion. Even at the largest stimulus level, the unadapted portion is less than 5% of the maximum rate. The parameter that has the strongest effect on the unadapted fraction is h_4. A five-fold increase in h_4 will decrease the unadapted fraction to an insignificant level at all the stimulus levels.

Figure 9 shows the response for a stimulus sequence of four steps, beginning with a step from 0 to 10^{-9}, followed by three 10-fold increases.

The computational results, using the parameters estimated in the Appendix, are shown in Figure 10. One sees that the response to the initial 10^{-9} M signal is too small compared to the experimental data. In order to get a significant initial response to a stimulus of 10^{-9} M, we changed the value of k_{-1} to 0.075, which is still in the range of the experimental values.

Figure 11 shows the response, and one can see that now it is very similar to the experimental data. Hereafter we will use this value, with other parameters unchanged, for the numerical experiments. A similar result can be obtained by slowing the rise of G_i' somewhat.

In Figure 9 the response to the second step of the stimulus sequence $H = 10^{-8}$ M is small compared to the responses to other stimulus levels. This can be reproduced in the model by speeding up the response of the inhibitory channel. For example, by increasing h_2 and h_5 by a factor of 3, one obtains a response very similar to that shown in Figure 9.

The simulations for a variety of stimuli are satisfactory using the parameter values given in Table 4, provided that k_1 is changed as above. This includes the response to a two-step sequential increase (Figure 12) and the two-step short time step stimulus (Figure 13). Experimental results and the simulation response curves are given here.

We conclude that the model can explain adaptation at the transduction level, using parameter estimates based on experimental observations in *Dd* and mammalian systems. In the following section we show that the model can also reproduce the observed oscillations in suspensions.

6. SIMULATION OF SUSPENSION EXPERIMENTS

Thus far we have only dealt with the modeling of perfusion experiments, in which case the extracellular cAMP is a specified function of time. As we have demonstrated elsewhere [32, 33], the dynamics of other experimental configurations can also be described with perhaps changes in one or two parameters, once the input–output behavior of the cells is accurately described by a model. In this section we demonstrate this for the present model by analyzing

the dynamics of suspensions. A detailed discussion of suspension experiments is given in [32].

6.1. SUSPENSION EXPERIMENTS AND A MATHEMATICAL MODEL

To describe the suspensions, we only have to append reactions for the extracellular dynamics and equations for the evolution of extracellular cAMP. The additional reactions arise from the presence of the extracellular enzymes.

$$\begin{aligned}
&\mathrm{cAMP}_o + \mathrm{mPDE} \underset{l_{-6}}{\overset{l_6}{\rightleftharpoons}} \mathrm{cAMP}_o - \mathrm{mPDE} \qquad (26)\\
&\mathrm{cAMP}_o - \mathrm{mPDE} \xrightarrow{l_7} \mathrm{AMP}\\
&\mathrm{cAMP}_o + \mathrm{ePDE} \underset{l_{-8}}{\overset{l_8}{\rightleftharpoons}} \mathrm{cAMP}_o - \mathrm{ePDE}\\
&\mathrm{cAMP}_o - \mathrm{ePDE} \xrightarrow{l_9} \mathrm{AMP}
\end{aligned}$$

Here cAMP_o denotes extracellular cAMP, mPDE denotes membrane-bound phosphodiesterase, cAMP_o–mPDE denotes the complex between cAMP and mPDE on the extracellular membrane, ePDE denotes the extracellular phosphodiesterase in solution, and cAMP_o–ePDE denotes the ePDE–cAMP_o complex in the extracellular solution. Notice that cAMP_o, is different from H and cAMP^*_o.

The additional differential equations are

$$\begin{aligned}
V_o\frac{dy_{14}}{dt} &= NV_c l_5 y_{12} + NA_c l_{-6} y_{15} + V_o l_{-8} y_{16} - NA_c l_6 y_{14} z_8 - NV_c l_8 y_{14} z_9 \qquad (27)\\
\frac{dy_{15}}{dt} &= -\left(l_{-6} + l_7\right) y_{15} + l_6 y_{14} z_8\\
\frac{dy_{16}}{dt} &= -\left(l_{-8} + l_9\right) y_{16} + l_8 y_{14} z_9 .
\end{aligned}$$

Here N denotes the total number of cells, V_o denotes the extracellular volume, and $A_c(V_c)$ denote the area (volume) per cell. In addition, y_{14} stands for [cAMP_o], y_{15} for [mPDE–cAMP_o,], y_{16} for [ePDE–cAMP_o], z_8 for free [mPDE], and z_9 for the free [ePDE]. In addition, there are two other conservation equations:

$$y_{15} + z_8 = [\mathrm{mPDE}]_T, \quad y_{16} + z_9 = [\mathrm{ePDE}]_T . \qquad (28)$$

The newly introduced variables y_{15} + y_{16} are both positive and bounded. In fact, we have

$$0 \leqslant y_{15} \leqslant [\mathrm{mPDE}]_T, \quad 0 \leqslant y_{16} \leqslant [\mathrm{ePDE}]_T .$$

It follows from this that $y14$ is also bounded.

By scaling the new independent variables and introducing additional nondimensional parameters, we obtain a nondimensionalized system for the u_i and v_i. Most of the equations are the same as in Section 7. The newly introduced dimensionless parameters and singular variables are listed in Table 12. We use the same scaling for y_{14} as y^*_{14}, $u_8 = y_{14}/[\text{iPDE}]_T$.

The newly introduced singular differential equations are

$$\epsilon_7 \frac{dv_7}{d\tau} = u_8 - v_7 - \frac{1}{\gamma_6} u_8 v_7, \quad (29)$$
$$\epsilon_8 \frac{dv_8}{d\tau} = u_8 - v_8 - \frac{1}{\gamma_8} u_8 v_8 .$$

As before, we set the time derivatives for the singular variables equal to zero, solve the resulting system, and use the results in the equatidns for the nonsingular variables. The result is that the new nonsingular variables satisfy the following system.

$$\frac{du_1}{d\tau} = \alpha_0 u_8 - (\alpha_0 u_8 + \alpha_1) u_1 + (\beta_5 - \alpha_0 u_8) u_6 - \beta_4 u_1 u_5, \quad (30)$$
$$\frac{du_4}{d\tau} = \beta_0 u_8 - (\beta_0 u_8 + \beta_1) u_4,$$
$$\frac{du_8}{d\tau} = \frac{\rho}{1-\rho}\left[\gamma_5 u_7 - \frac{\gamma_7 u_8}{u_8 + \gamma_6} - \frac{\gamma_9 u_8}{u_8 + \gamma_9}\right]$$

Here ρ is the ratio of cell volume to the total volume in an experiment, that is,

$$\rho = NV_c/(NV_c + V_o).$$

Using the parameter values given in the Appendix, we obtain the values for the dimensionless parameters given in Table 13.

6.2. NUMERICAL SIMULATION OF SUSPENSION EXPERIMENTS

We have tested the model numerically both for the scaled system and the unscaled system. As is expected from the singular perturbation analysis, the simplified system approximates the original system very well.

There are three types of qualitatively distinct dynamics in suspensions, depending on the parameter values chosen: (1) adaptation without oscillation, (2) decaying oscillations, and (3) stable oscillations. A typical response curve for each of the last two types is shown in Figure 14.

Since there are many parameters involved in the system, a complete demarcation of parameter space according to the type of response is difficult to obtain. However, if we keep

certain variables fixed and let only one variable change, we can do a bifurcation analysis. Bifurcation analysis with respect to certain parameters that are known to change in different developmental stages (such as total amount of adenylate cyclase and the cAMP secretion rate) gives insight into how the dynamics change with the developmental stage. The results of this type of analysis were given in [32]. Here we simply illustrate that the experimentally observed oscillations can be reproduced with the model. Figure 15 shows (a) the experimental results and (b) the numerical results. One sees that the latter correspond well with the experimental data in both magnitude and frequency.

The peak amplitude of the extracellular cAMP is very sensitive to the amount and the turnover rate of adenylate cyclase and to the activity of iPDE and mPDE. Figure 16 shows how a change of the values of mPDE and $\gamma 5$ changes the magnitude of the response.

On the other hand, the frequency of the oscillation is very sensitive to $\beta 2 \equiv h_2[G_i]_T/k_5$ and $\beta_5 = h_5/k_5$. Figure 17 shows how the frequency can be changed by proportional changes in β_2 and β_5, which determine the slowest process in the system (see Appendix for the explanation).

7. EXPERIMENTAL TESTS OF THE MODEL

7.1. PROPOSED EXPERIMENTS

In this section we propose several experiments that can be used to test the model, and we describe the predictions made by the model for these experiments.

The effect of cholera toxin on adaptation of the relay response in *Dictyostelium discoideum* has not yet been reported. However, if we assume that cholera toxin acts on the G_s of *Dd* in the same way it acts on G_s in other cells, then it will block hydrolysis of activated G_s. When the agonist and antagonist are different, as in many other systems, the result of exposure to cholera toxin is that all of the UC is eventually converted into AC in the presence of a prolonged agonist signal. However, in *Dd* the agonist and antagonist are the same, and thus both signals arrive at the same time. As a result, in our model most of the HR_s complex is split rapidly, and only a small amount of adenylate cyclase is activated in a short time. Thus a small stimulus cannot turn on all the adenylate cyclase in a short time, and a further increase in the stimulus will cause a further increase in the AC activity. An interesting prediction of our model under cholera toxin treatment is the following.

Suppose that the external cAMP concentration is held at S_0 until time T_0 and that the amount of AC turned on is A_0 (see Figure 18). Next increase the external cAMP concentration by S_1 and hold it until T_1, and suppose that the corresponding increase of AC is A_1. Then the model predicts that for an external cAMP concentration of $S_0 + S_1$, the corresponding amount of adenylate cyclase that is activated for times of the order of T_1 will be $A_0 + A_1$, that is, the amount of AC activated is additive in a quasi-steady state. Since adaptation is not complete, the presence of some unadapted HR_s will eventually activate all the AC. However, the increase in AC activity due to the residual HR_s is slow, and the additivity should be observable on the experimental time scale. This prediction can be used to check our model.

Since we do not know whether cholera toxin interacts with G_s in *Dd*, we propose another experiment to check this model. If we use a nonhydrolyzable substitute such as GTPγS or Gpp[NH]p for GTP, activated AC will not be deactivated, just as in the case of cholera toxin treatment. On the other hand, the signal is also changed in the inhibitory pathway. A prolonged stimulus will result in the complete activation of G_i, and this will turn off further activation of AC. The pseudo-steady-state concentrations of G_s' and AC will be proportional to the stimulus level and will not decay.

The essential difference between the response of cholera toxin-treated cells and cells treated with GTPγS is in the response to a second cAMP signal of higher concentration. While the cholera toxin-treated cell should have the property of semiadditivity on a short time scale, the cells treated with GTPγS should have no response to the sequential increase of stimulus. Very little of the second stimulus will pass the receptor level, since most of the G_i is activated by the first signal. The newly generated population of HR_s will rapidly be bound with a_i-GTPγS and thus will not catalyze the transition from G_s to G_s'. When Gpp[NY]p is used instead of GTPγS the time course of the response will be essentially the same, but there will be a slight decrease in the magnitude of the response because the affinity of a_i and a_s for Gpp[NH]p is not as high.

These two tests are not able to distinguish between our model and a model with direct inhibitory interaction between G_i' and $G_s' - AC$. Both predict the same type of response for the two experiments. However, there is an experiment that can rule out the possibility of a direct interaction model, and this hinges on the possibility of measuring the activated G_s' concentration.

In the direct interaction inhibition model, the fraction of G_s activated will remain large under a constant stimulus. On the other hand, if adaptation occurs at the receptor level, as in our model, then after an initial burst following a step change in the stimulus, the fraction of G_s will return to a low level fixed by the stimulus, If it is possible to measure the time course of G_s' in the membrane, then the two models can be distinguished.

In the next section, we report the detailed predictions made by the model for these experiments.

7.2. NUMERICAL OUTPUTS FOR THE EXPERIMENTS

The first numerical experiment we do concerns the pertussis toxin-treated cells. The effect of pertussis toxin is simulated by letting $h_2 = 0$, which means that G_i cannot be activated. The numerical simulation predicts a near-linear increase in the total amount of cAMP secreted. This differs from the experimental result in [39]. The decrease in the cAMP secretion rate in the experiment results from the phosphorylation of receptors, which is not included in our model.

To simulate the effect of treatment with cholera toxin, we let $k_5 = 0$. Notice that here we cannot use the scaled system for the numerical experiment, because in that system k_5 is used to scale the time. The numerical output from the nonscaled system (5)–(8) is shown in

Figure 19. The figure should be compared with Figure 18 to check the steady-state additivity property in this experiment. Notice that in Figure 18a, adaptation does occur at receptor level, but G'_s does not decay.

If GTPγS is used instead of GTP, then both G'_s and G'_i are nonhydrolyzable. We mimic this by letting $k_5 = h_5 = 0$. The numerical output is shown in Figure 20. We see here that the first signal ($H = 0.1\ \mu$M) can turn on almost all the G'_i after a certain time. The high level of G'_i blocks the response of the system to the second stimulus ($H = 1\ \mu$M). The small increase in internal cAMP concentration and the increased secretion rate are due to the unadapted portion of HR_s, which is very small.

8. CONCLUSIONS

We have developed a model for adaptation of the relay response in *Dictyostelium discoideum* and have shown that it can reproduce the experimental results available for perfusion and suspension experiments. As in the Monk-Othmer model, this has been done using the same parameters to model both perfusion and suspension experiments, except for those that are known to vary with developmental age. It was shown in [32], [33] that several modifications to the basic model presented there, such as the inclusion of time delays in the stimulus and adaptation pathways, do not alter the general conclusions reached, and the same conclusion undoubtedly applies here, although we have not checked this in detail. Certain aspects, such as the rise time of the production and secretion of cAMP, could be improved by tuning the parameters, but that is of secondary importance.

As we mentioned in Section 2.2, another possible mechanism for adaptation is based on direct interaction between G'_i and G'_sAC. This would require a second G_i protein binding site on adenylate cyclase, such that when it is occupied with G'_i the activity of the cyclase is essentially zero. A kinetic scheme for this mechanism is as follows.

$$\begin{aligned} &G'_s + UC \rightleftharpoons G'_sAC \\ &G'_sAC + G'_i \rightarrow G'_sAC - G'_i \\ &G'_sAC - G'_i \rightarrow \alpha_s GDP + UC + G'_i \\ &G'_sAC - G'_i \rightarrow G'_sAC + \alpha_i GDP \end{aligned} \tag{31}$$

Our numerical simulations indicate that an adaptation model based on this mechanism can also reproduce the experimental observations in perfusion experiments. We have not checked this for the suspension experiments, but past experience indicates that it will function properly in that context as well. A model based on direct interaction of G'_i with the cyclase is similar in spirit to the Monk-Othmer model, wherein calcium plays the inhibitory role and interacts directly with the cyclase.

At present one cannot discriminate on theoretical grounds between the direct inhibition model described in this section and the model proposed and analyzed in this paper. However, the fact that a G'_i–cyclase complex has not been found in other systems favors the latter

model. Energetic considerations also favor the latter model, since adaptation at the level of the cyclase entails approximately twice the consumption of GTP in the presence of a constant signal. However, the final determination of a model hinges on identifying the details of the biochemical pathways from extracellular signal to cyclase.

A number of other models for cyclic AMP control and synthesis in *Dictyostelium* have appeared, and these were reviewed in [32] and [33]. Models involving receptor modification are motivated by the experimental fact that cAMP induces phosphorylation of the cAMP receptors in *Dd* [24,25] and that this occurs on the same time scale as adaptation. Thus phosphorylation may be involved in adaptation, perhaps by interfering with the activation of a G_s protein. However, as we mentioned earlier, phosphorylation is not sufficient for adaptation, since pertussis toxin treatment blocks adaptation but does not interfere with receptor modification [40, 50]. This suggests that activation of a G_i protein is necessary for adaptation [42]. In this paper we developed a mechanism based on this and showed that it can produce the observed adaptation. We have not incorporated a role for phosphorylation, but this is easily done and would not alter the basic conclusions, since it simply introduces alternative pathways for the intermediates, and the same dynamics are as predicted by the present model can be obtained by retuning the rate constants.

The model presented in this paper concerns only the relay response. However, cyclic AMP stimuli also trigger a chemotactic response, and to model the cellular response more completely we would have to incorporate cyclic GMP and perhaps other species [48]. Such a model is presently under development.

Acknowledgments

This research was supported in part under NIH grant GM29123.

APPENDIX

In this appendix, we estimate the model parameters.

A.1.: REACTION KINETIC CONSTANTS

Two classes of cAMP binding sites have been identified in relay competent *Dd* cells, which are denoted as the A site and B site [50]. The total number of sites is approximately (5–10) $\times 10^4$ per cell [18]. The B sites comprise only about 4% of all binding sites, and it is believed that they are involved in the cGMP and chemotaxis pathways. We take the upper value of 10^5 receptors per cell for the total binding sites, that is, 9.6×10^4 for A sites. Of the A sites, about 40% are fast dissociation with high affinity (K_d = 60 nM), and about 60% are fast dissociation with low affinity (K_d = 450 nM). It is reasonable to assume that the high-affinity receptors of the A site are R_s and the low affinity ones are R_i, since usually $G_i > G_s$. The values of the binding and dissociation constants for the two receptor types are estimated as

$$k_1 = 7.5\text{s}^{-1}\mu\text{M}^{-1}, \quad k_{-1} = 0.45\text{s}^{-1}$$
$$h_1 = 2.2\text{s}^{-1}\mu\text{M}^{-1} \quad h_{-1} = 1.0\text{s}^{-1}$$

in [49].

Data on the rate of activation of G_s are reported in terms of the rate constant

$$k_{\text{on}} \equiv \frac{k_2 k_3}{k_{-2} + k_3}\left[\text{HR}_s\right].$$

Levitzki [29] reported that k_{on} is in the range of 0.5–1.5 min^{-1} for mammalian cells. Freissmuth et al. [19] reported a higher k_{on}, with a minimum of 2 min^{-1}. The latter estimate is more compatible with the observed rates of cAMP secretion in *Dd* (the secreted cAMP reaches its peak at about 1.5 min). There is no measurement of k_{on} reported for *Dd*, so we will take the value of $k_{\text{on}} = 2.5\ \text{min}^{-1} = 0.0167\ \text{s}^{-1}$. Since

$$k_{\text{on}} = \frac{k_2 k_3}{k_{-2} + k_3}\left[\text{HR}_s\right] = \frac{k_2 k_3}{k_{-2} + k_3}\left(\frac{[\text{H}]\left[\text{R}_s\right]_T}{[\text{H}] + \left[\text{R}_s\right]_T}\right),$$

the value of k_{on} depends on the stimulus level. From this estimate for k_{on} we have to estimate k_2, k_{-2}, and k_3. If we assume an intermediate stimulus level of $[\text{H}] \sim 10^{-2}\ \mu\text{M}$, we have $[\text{HR}_s]/[\text{R}_s]_T \sim 0.1$, and therefore

$$\frac{k_{\text{on}}}{\left[\text{R}_s\right]_T} = \frac{0.1 k_2 k_3}{k_{-2} + k_3}.$$

The value for k_3 is reported as $10^4\ \text{s}^{-1}$ in [19]. We still cannot obtain both k_2 and k_{-2}, and therefore we assume that $k_{-2} \ll k_3$. This means that the rate of dissociation of HR_sG_s is small compared with the rate of production of G_s', and with this assumption we obtain

$$k_2 = 10 k_{\text{on}} / \left[\text{R}_s\right]_T = 1000.0\ \text{m}^2/(\mu\text{mol} \cdot \text{s}).$$

The analysis for the estimation of h_2, h_{-2}, and h_3 is very similar to that of h_2, h_{-2}, h_3 but here there is no reported value of h_{on}. We can, however, use the cAMP secretion to estimate these kinetic constants. A typical value for the peak value of cAMP secretion is $t^{\text{peak}} \sim 1.5$ min, and we assume that the half-time of the inhibitory signal is

$$t^i_{0.5} = 1.5 t^{\text{peak}} = 1.5 \times 1.5 = 2.25\ \text{min}.$$

Knowing $t^i_{0.5}$, we can get an estimate of h_{on} from the dynamics of this pathway. Under the assumption of a pseudo-steady state, we have

$$h_{\text{on}} = (\ln 2)/t^i_{0.5} = 5.13 \times 10^{-3}\ \text{s}^{-1}.$$

If we assume that the stimulus level to yield this value of h_{on} is $[HR_i]/[R_i]_T \sim 0.5$, then we can get an estimate for h_2, h_{-2}, and h_3 in the same way as previously. The result is that

$$h_2 = \frac{1}{0.5}\left(\frac{0.01}{[R_i]_T}\right) = 40\ \mathrm{m}^2/(\mu\mathrm{mol}\cdot\mathrm{s}),$$

$h_{-2} = 0\ \mathrm{s}^{-1}$, and $h_3 = 400\ \mathrm{s}^{-1}$.

Next we set k_4 and h_4. Based on the observation that the rate of production of cAMP is first-order in the receptor concentration, Levitzki argued that G_s is precoupled to the inactivated adenylate cyclase [27]. However, as we noted in the text, there is evidence that suggests that G_s shuttles between HR_s and adenylate cyclase. Whichever is correct, it is safe to assume, in the absence of *Dd*–specific information, that k_4 is large, and we use the value $k_4 = 1 \times 10^4$ $\mathrm{m}^2/(\mu\mathrm{mol}\cdot\mathrm{s})$ for the numerical computations. For the same reasons we can assume that h_4 is very large, that is, that the affinity of G_i' to HR_s is very high, and in the numerical experiments we use $k_4 = 5 \times 10^5\ \mathrm{m}^2/(\mu\mathrm{mol}\cdot\mathrm{s})$.

There is uncertainty concerning the rate of hydrolysis of the activated G_s protein as well. Levitzki reports that k_{off} ($\equiv k_5$) is in the range of 13–15 min^{-1} [28], but Casey and Gilman [7] report a value of k_{off} of around 3 min^{-1}. For the numerical computations we use the value $k_5 = 3.75\ \mathrm{min}^{-1} = 0.0625\ \mathrm{s}^{-1}$.

The rate of decay of G_i' is the slowest step involved in the oscillations in suspension experiments. Restimulation can only occur after G_i' has decayed to a low-level, which means that the period of the oscillations depends strongly on h_{off}. If we assume that the external cAMP is suddenly withdrawn from the extracellular medium, it will take about 4 half-lives of G_i' to degrade ~ 95% of existing G_i'. However, extracellular cAMP is degraded only gradually by ePDE and mPDE, and thus the actual time for sufficient degradation of G_i' may be severalfold longer than if the signal is abruptly terminated. The observed time period for oscillation is about 10 min [38]. If we assume that the time is 1.5–1.75 times longer and note that

$$t^{0.5} = (\ln 2)/h_{off}$$

and

$$(1.5 - 1.75) \times 4 \times t^{0.5} = 10\ \mathrm{min} = 600\ \mathrm{s},$$

we find that

$$6.94 \times 10^{-3}\mathrm{s}^{-1} < h_{off} < 8.0 \times 10^{-3}\mathrm{s}^{-1}.$$

We take a value of

$$h_{\text{off}} = h_5 = 7.5 \times 10^{-3} \text{s}^{-1}.$$

The rate of association between the $\beta\gamma$ subunit and the hydrolyzed G proteins is set at

$$k_6 = h_7 = 10^5 \text{ m}^2/(\mu\text{moles} \cdot \text{s}).$$

This assumption is based on the known fact that α-GDP has a high affinity for $\beta\gamma$ [21].

There is some experimental data that can be used for the estimation of h_6. van Haastert and de Wit [49] report that the high-affinity receptors are transformed to low-affinity receptors in the presence of prolonger stimuli. The interpretation of this in the context of our model is that HR_sG_i' has a much lower affinity for H then does R_s. There is no transformation between the two different binding sites R_s and R_i in our model; the transformation from high affinity to low affinity is due to the reaction

$$HR_sG_i' \xrightarrow{h_6} H + R_s + G_i'.$$

It follows that the coupling of h_6 with k_1 should yield the same value of the affinity as for the low-affinity sites, which implies that

$$h_6/k_1 = h_d = h_{-1}/h_1.$$

From this we obtain

$$h_6 = (1.0/2.2)7.5 = 3.4 \text{ s}^{-1}.$$

The actual value of h_6 we used is

$$h_6 = 17.0 \text{ s}^{-1}.$$

Finally, we have to estimate the constants for adenylate cyclase, internal phosphodiesterase, and the secretion rate. It is reported in [29] that the typical value for the turnover number of activated adenylate cyclase is

$$l_{\text{cat}} = 1100 \text{ min}^{-1} = 18.4 \text{ s}^{-1}$$

provided the concentration of ATP is held constant. Under this condition, we have that

$$l_{\text{cat}} = l_1 l_2 / \left(l_{-1} + l_2 \right).$$

Since this process is fast, the selection of l_1, l_{-1}, l_2 has little effect on the dynamics on the time scale we focus on, provided that the combination of the chosen values of l_1, l_{-1}, l_2 yields the correct value of l_{cat}. Thus we take $l_1 = l_{-1} = 20.2\ \text{s}^{-1}$ and $l_2 = 202\ \text{s}^{-1}$.

The kinetic constants for iPDE have been estimated from experiments in [32] and [37]. It is reported there that the Michaelis-Menten constants are

$$V_{\text{iPDE}}^{\max} = l_4 [\text{iPDE}]_T = 86.67\ \mu\text{M/s}$$

and

$$K_{\text{iPDE}} = \left(l_{-3} + l_4 \right) / l_3 = 10\ \mu\text{M}.$$

The individual value for each of the constants involved is unknown, but it is reasonable to assume that the turnover number of iPDE is not very high, since the function of iPDE is to hydrolyze excess cAMP so as to control the internal level of cAMP. For simplicity we take $l_{-3} = 0\ \text{s}^{-1}$ and $l_4 = 50\ \text{s}^{-1}$, and then we can get

$$l_3 = 5\ \mu\text{M}^{-1}\ \text{s}^{-1} = 5 \times 10^{-3}\ \text{m}^3/(\mu\text{mol} \cdot \text{s}),$$
$$[\text{iPDE}]_T = 1.7334\ \mu\text{M} = 1.7334 \times 10^3\ \mu\text{mol/m}^3$$

Finally, it is reported in [11] that l_5 ranges from $0.34\ \text{min}^{-1}$ to $0.94\ \text{min}^{-1}$. We use the intermediate value

$$l_5 = 0.84\ \text{min}^{-1} = 0.014\ \text{s}^{-1}.$$

A.2.: CELL GEOMETRY AND CHEMICAL CONCENTRATIONS

The typical cell radius for *Dd* is 11 μm [6, 37]. If a spherical geometry is assumed, then

$$V_c = 696.9\ \mu\text{m}^3 \quad \text{and} \quad A_c = 380.1\ \mu\text{m}^2$$

Concentrations are stated either per unit area or per unit volume. These can be converted to molecules per cell as follows:

$$y_i(\text{molecules/cell}) = 2.29 \times 10^8 y_i\left(\mu\text{mol/m}^2\right),$$
$$y_i(\text{molecules/cell}) = 4.20 \times 10^2 y_i\left(\mu\text{mol/m}^3\right).$$

Therefore

$$[\text{iPDE}]_T = 1.7334\ \mu\text{M} = 7.28 \times 10^5\ \text{molecules/cell}$$

and

$$\begin{aligned}\left[\text{R}_\text{s}\right] &\doteq 0.4 \times 9.6 \times 10^4 = 3.84 \times 10^4\ \text{milecules/cell},\\ \left[\text{R}_\text{i}\right] &\doteq 0.6 \times 9.6 \times 10^4 = 5.76 \times 10^4\ \text{milecules/cell}.\end{aligned}$$

At present there is little information about the concentrations of G_s and G_i. It is commonly claimed that the concentration of G proteins is higher than the concentration of receptors, and one estimate for mammalian cells give a value for G_s of 100,000 per cell [1]. It is believed that in *Dd* the number of G protein molecules is in the same range as that of receptors [39], and we take them as equal in our model. Thus

$$\left[\text{G}_\text{s}\right] = 3.84 \times 10^4/\text{cell} \quad \text{and} \quad \left[\text{G}_\text{i}\right] = 5.76 \times 10^4/\text{cell}.$$

The total amount of adenylate cyclase is equal to the concentration of G_s in some mammalian cells [29] (but not others, cf. [1]), and we assume that this is true in *Dd* as well. Thus we have

$$[\text{UC}]_T = 3.48 \times 10^4\ \text{molecules/cell},$$

and the corresponding concentrations are

$$\begin{aligned}\left[\text{R}_\text{s}\right]_T &= 1.67 \times 10^{-4}\ \mu\text{mol/m}^2, \quad \left[\text{R}_\text{i}\right]_T = 2.50 \times 10^{-4}\ \mu\text{mol/m}^2\\ \left[\text{G}_\text{s}\right]_T &= 1.67 \times 10^{-4}\ \mu\text{mol/m}^2, \quad \left[\text{G}_\text{i}\right]_T = 2.50 \times 10^{-4}\ \mu\text{mol/m}^2\end{aligned}$$

and

$$[\text{UC}]_T = 1.67 \times 10^{-4}\ \mu\text{mol/m}^2.$$

This assumption is not critical, for we set the overall production rate to match the observed concentrations and secretion rates.

A.3.: PARAMETERS IN THE SUSPENSION EXPERIMENTS

The new parameters that must be estimated for the suspension experiments are $V_{\text{max}}^{\text{mPDE}}$, K_{mPDE}, $V_{\text{max}}^{\text{ePDE}}$, and K_{ePDE}, where

$$V_{\max}^{\mathrm{mPDE}} = l_7[\mathrm{mPDE}]_T, \quad K_{\mathrm{mPDE}} = \left(l_{-6} + l_7\right)/l_6, \quad \text{(A1)}$$

$$V_{\max}^{\mathrm{ePDE}} = l_9[\mathrm{ePDE}]_T, \quad K_{\mathrm{ePDE}} = \left(l_{-8} + l_9\right)/l_8\,. \quad \text{(A2)}$$

The values of these parameters have been estimated in [32] and [37].

$$V_{\max}^{\mathrm{mPDE}} = 1.67 \times 10^6 \text{ molecules/(cell} \cdot \text{s)} = 7.29 \times 10^{-3}\ \mu\text{mol}^{-1}\ \text{m}^{-2},$$
$$K_{\mathrm{mPDE}} = 0.5\ \mu\text{M},$$
$$V_{\max}^{\mathrm{ePDE}} = 3 \times 10^7 \text{ molecules/(cell} \cdot \text{s)} = 7.15 \times 10^4\ \mu\text{mol}^{-1}\ \text{m}^{-3},$$
$$K_{\mathrm{ePDE}} = 1.3\ \text{mM}\,.$$

In the numerical simulations, we used $K_{\mathrm{mPDE}} = 5.0\ \mu$M, $V_{\max}^{\mathrm{mPDE}} = 4.48 \times 10^{-2}\ \mu\text{mol}^{-1}\ \text{m}^{-2}$, $K_{\mathrm{ePDE}} = 1.3$ mM, and $V_{\max}^{\mathrm{ePDE}} = 4.39 \times 10^5\ \mu\text{mol}^{-1}\ \text{m}^3$.

REFERENCES

1. Adawia A, Jasper JR, I'. A Insel, and H. J. Motulsky, Stoichiometry of receptor-G_s-adenylate cyclase interactions, FASEB J 52300–2303 (1991).
2. Arad H, Rosenbusch JP, and Levitzki A, Stimulatory GTP regulatory unit N_s and catalytic unit of adenylate cyclase are tightly associated: mechanistic consequences, Proc. Natl. Acad. Sci. USA 81:6579–6583 (11 1982).
3. Asano T, Katada T, Gilman A, and Ross E, Activation of the inhibitory GTP-binding protein of adenylate cyclase, G_i, by β-adrenergic receptors in reconstituted phospholipid vesicles, J. Biol. Chem 259(1.5):9351–9354 (1984). [PubMed: 6146612]
4. Berridge M, Inositol trisphophate and diacylglycerol: two interacting second messengers, Ann. Rev. Biochem 56:159–193 (1987). [PubMed: 3304132]
5. Bominaar A, Snaar-Jagalska B, Kesbeke F, and van Haastert P, Signal-transducing G proteins in *Dictyostelium discoideum*, in the guanine nucleotide binding proteins Common structural and functional properties (NATO ASI, Vol. 165) Bosch L, et al. eds., Springer-Verlag, Berlin, 1989, pp. 369–375.
6. Brachet P and Klein C, Inhibition of growth and cellular aggregation of *Dictyostelium discoideum* by steroid compounds, Exp. Cell Res 93:159–165 (1975). [PubMed: 124657]
7. Casey PJ and Gilman AG, G protein involvement in receptor-effector coupling, J. Biol. Chem 263(6):2577–2580 (1988). [PubMed: 2830256]
8. Devreotes P, *Dictyostelium discoideum*: a model system for cell-cell interactions in development, Science 245:1054–1058 (9 1989). [PubMed: 2672337]
9. Devreotes PN and Steck TL, Cyclic 3',5' AMP relay in *Dictyostelium discoideum* II. Requirements for the initiation and termination of the response, J. Cell Biof 80:300–309 (1979).
10. Devreotes PN, Derstine PL, and Steck TL, Cyclic 3',5' AMP relay in *Dictyostelium discoideum* I. A technique to monitor responses to controlled stimuli, J. Cell Biol 80:291–299 (1979). [PubMed: 222769]
11. Dinauer MC, MacKay SA, and Devreotes PN, Cyclic 3',5' AMP relay in *Dictyostelium discoideum* III. The relationship of cAMP synthesis and secretion during the cAMP signaling response, J. Cell Biol 86:537–544 (1980). [PubMed: 6249825]

12. Dinauer MC, Steck TL, and Devreotes PN, Cyclic 3',5' AMP relay in *Dictyostelium discoideum* IV. Recovery of the cAMP signaling response after adaptation to cAMP, J. Cell Biol 86:545–553 (1980). [PubMed: 6249826]
13. Dinauer MC, Steck TL, and Devreotes PN, Cyclic 3',5' AMP relay in *Dictyostelium discoideum* V. Adaptation of the cAMP signaling response during cAMP stimulation, J. Cell Biol 86:554–561 (1980). [PubMed: 6249827]
14. Ehlert FJ, The relationship between muscarinic receptor occupancy and adenylate cyclase inhibition in the rabbit myocardium, Mol. Pharmacol 28: 410–421 (1985). [PubMed: 4058422]
15. Europe-Finner G and Newell P, Inositol 1,4,5-trisphophate induces GMP formation in *Dictyostelium discoideum*, Biochem. Biophy. Res. Commun 130(3): 1115–1122 (1985).
16. Europe-Finner G and Newell P, Cyclic AMP stimulates accumulation of inositol trisphosphate in *Dictyostelium*, J. Cell Sci 87:221–229 (1987). [PubMed: 2821026]
17. Europe-Finner G, Gammon B, Wood C, and Newell P, Inositol tris- and polyphosphate formation during chemotaxis of *Dictyostelium*, J. Cell Sci 93: 585–592 (1989). [PubMed: 2558121]
18. Firtel RA, van Haastert PJM, Kimmel AR, and Devreotes PN, G protein linked signal transduction pathways in development: *Dictyostelium* as an experimental system, Cell 58:235–239 (7 1989). [PubMed: 2546676]
19. Freissmuth M, Casey PJ, and Gilman AG, G proteins control diverse pathways of transmembrane signaling, FASEB J 3:2125–2131 (8 1989). [PubMed: 2546847]
20. Gerisch G and Wick U, Intracellular oscillations and release of cyclic AMP from *Dictyostelium* cells, Biochem. Biophys. Res. Commun 65:364–370 (1975). [PubMed: 167769]
21. Gilman AG, G proteins: transducers of receptor-gated signals, Ann. Rev. Biochem 56:615–649 (1987). [PubMed: 3113327]
22. Janssens P and van Haastert P, Molecular basis of transmembrane signal transduction in *Dictyostelium discoideum*, Microbial. Rev 51(4):396–418 (1987).
23. Kesbeke F, van Haastart P, and De Wit R, Chemotaxis to cyclic AMP and folic acid is mediated by different G proteins in *Dictyostelium discoideum*, J. Cell Sci 961669–673 (1990).
24. Klein P, Knox B, Borlies J, and Devreotes P, Purification of the surface cAMP receptor in *Dictyostelium*, J. Biol. Chem 261:352–357 (1987).
25. Klein P, Vaughn R, Borlies J, and Devreotes P, The surface cAMP receptor in *Dictyostelium*, J. Biol. Cem 262:358–364 (1987).
26. Levitzki A, Receptors: A Quantitative Approach, Benjamin/Cummings, Menlo Park, Calif, 1984.
27. Levitzki A, β-adrenergic receptors and their mode of coupling to adenylate cyclase, Physiol. Rev 66(3):819–854 (1986). [PubMed: 3016770]
28. Levitzki A, From epinephrine to cyclic AMP, Science 24:800–806 (1988).
29. Levitzki A, Transmembrane signaling to adenylate cyclase in mammalian cells *Saccharomyces cerevisiae*, TIBS 13:298–301 (1988). [PubMed: 2856454]
30. Limbird LE, Activation and attenuation of adenylate cyclase, Biochem. J 195:1–13 (1981). [PubMed: 6272740]
31. Marbach S, Shiloach J, and Levitzki A, G_i affects the agonist-binding properties of β-adrenoceptors in the presence of G_s, Eur. J. Biochem. FEBS, pp. 239–246 (1988).
32. Monk PB and Othmer HG, Cyclic AMP oscillations in suspensions of *Dictyostelium discoideum*, Phi. Trans. Roy. Sot. Lond 323(1215):185–224 (1989).
33. Monk PB and Othmer HG, Wave propagation in aggregation fields of *Dictyostelium discoideum*, in Lectures on Mathematics in the Life Sciences, Othmer HG, Ed., Ann. Math. Sot., Providence, R.I., 1989.
34. Othmer HG and Monk PB, Concentration waves in aggregation fields of a cellular slime mold, in Biomathematics and Related Computational Problems, Ricciardi L, Ed., Kluwer, Dordrecht, 1988, pp. 381–398.
35. Othmer HG, Monk PB, and Rapp PE, A model for signal relay and adaptation in *Dictyostelium discoideum*. Part II. Analytical and numerical results, Math. Biosci 77:77–139 (1985).
36. Rapp PE, Monk PB, and Othmer HG, A model for signal relay and adaptation in *Dictyostelium discoideum*. Part I. Biological processes and the model network, Math. Biosci 77:35–78 (1985).

37. Rapp PE, Monk PB, and Othmer HG, Quantitative estimates of kinetic parameters in the calcium cyclic nucleotide network in *Dictyostelium discoideum*, Tech. Rep, Department of Physiology and Biochemistry, Medical College of Pennsylvania, Philadelphia, 1985.
38. Roos W, Scheidegger C, and Gerisch G, Adenylate cyclase activity oscillations as signals for cell aggregation in *Dictyostelium discoideum*, Nature 266:259–260 (1977). [PubMed: 191758]
39. Snaar-Jagalska E and van Haastert PJM, Pertussis toxin inhibits cAMP-induced desensitization of adenylate cyclase in *Dictyostelium discoideum*, Mol. Cell. Biochem 92:177–189 (1990). [PubMed: 2155382]
40. Snaar-Jagalska BE, Devreotes PN, and Van Haastert PJM, Ligand-induced modification of a surface cAMP receptor of *Dictyostelium discoideum* does not require its occupancy, J. Biol. Chem 263:897–901 (1988). [PubMed: 2826466]
41. Snaar-Jagalska BE, Kesbeke F, and Van Haastert PJM, G-proteins in the signal transduction pathways of *Dictyostelium discoideum*, Dev. Genet 9:215–226 (1988).
42. Snaar-Jagalska E, Van Es S, Kesbeke F, and van Haastert PJM, Activation of pertussis toxin-sensitive guanine-nucleotide binding regulatory protein during desensitization of *Dictyostelium discoideum* cells to chemotactic signals, Eur. J. Biochem 195:715–721 (1991). [PubMed: 1847868]
43. Stryer L, proteins G: a family of signal transducers, Ann. Rev. Cell Biol 2:391 (1986). [PubMed: 3103658]
44. Stryer L, Biochemistry, 3rd ed, W. H. Freeman, New York, 1988.
45. Taylor CW, The role of G proteins in transmembrane signalling, Biochem. J 272:1–13 (1990). [PubMed: 2176077]
46. Tolkovsky A, Braun S, and Levitzki A, Kinetics of interaction between β-receptors, GTP protein, and catalytic unit of turkey erythrocyte adenylate cycles, Proc. Natl. Acad. Sci. USA 79:213–217 (1 1982). [PubMed: 6281756]
47. Tota MR and Schimerlik MI, Partial agonist effects on the interaction between the atria1 muscarinic receptor and the inhibitory guanine nucleotide-binding protein in a reconstituted system, Mol. Phurmucol 37:996–1004 (1990).
48. van Haastert PJM and Konijn TM, Signal transduction in the cellular slime molds, Mol. Cell. Endocrinol 2611–17 (1983).
49. van Haastert PJM and de Wit RJ, Demonstration of receptor heterogeneity and affinity modulation by nonequilibrium binding experiments, J. Biol. Chem 259(21):13321–13328 (1984). [PubMed: 6092374]
50. van Haastert PJM, de Wit RJW, Janssens PMW, Kesbeke F, Snaar-Jagalska BE, Van Lookeren MM, and Konijn TM, Adaptation of *Dictyostelium discoideum* cells to chemotactic signals, in Molecular Mechanisms of Desensitization to Signal Molecules (NATO ASI Vol. 6), Konijn TM, et al., Eds., Springer-Verlag, Berlin, 1987, pp. 25–42.

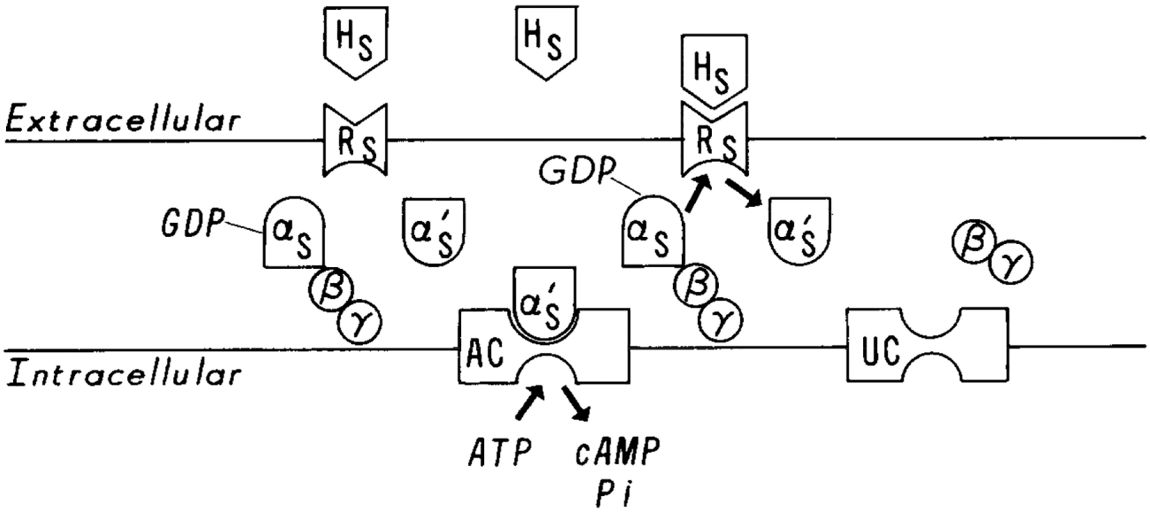

FIG. 1.

A schematic diagram of the activation of adenylate cyclase via G_s proteins. H_s denotes the stimulus signal, R_s the stimulus receptor, α_sGDP$\beta\gamma$ unactivated G_s protein, and UC unactivated adenylate cyclase. It is believed that upon binding of H_s with R_s, G_s is activated by the H_sR_s complex. This involves the release of the $\beta\gamma$ subunits and the addition of GTP to the α_s chain. α_sGTP, which is denoted by α'_s in this figure, then activates adenylate cyclase, which catalyzes the conversion of ATP to cAMP.

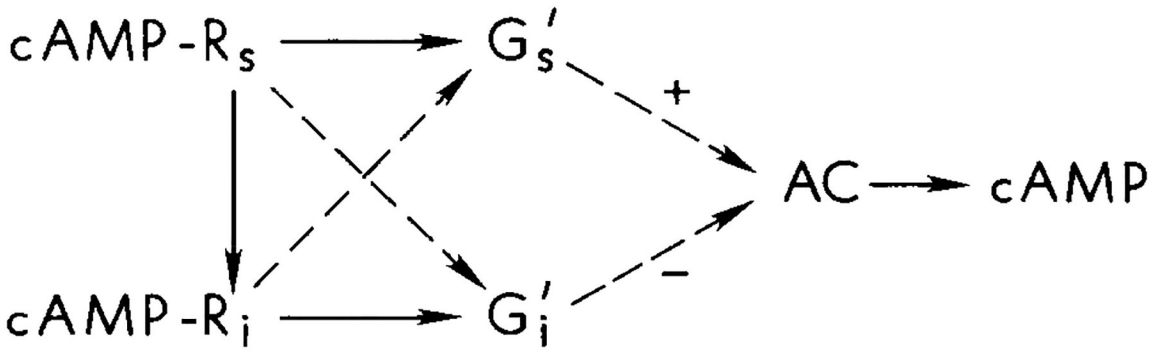

FIG. 2.

The scheme of interactions for the regulation of AC proposed by van Haastert and coworkers [39–41].

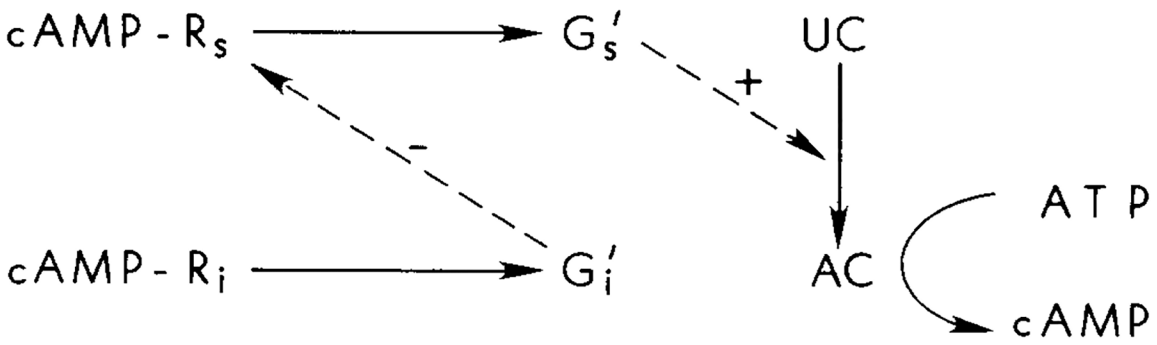

FIG. 3.

A schematic diagram of the interactions in the proposed model. An extracellular cAMP stimulus serves as both the stimulus and the inhibitory signal. Adaptation arises from the action of G_s' on the hormone–receptor cmplex. Viewed at the level of cAMP production, this interaction produces a feedforward mechanism for the control of cAMP production.

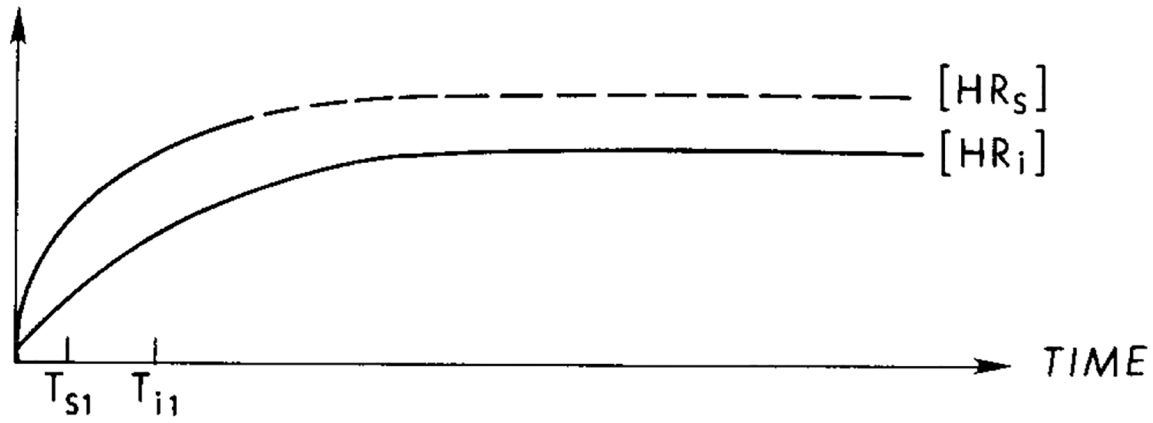

(a)

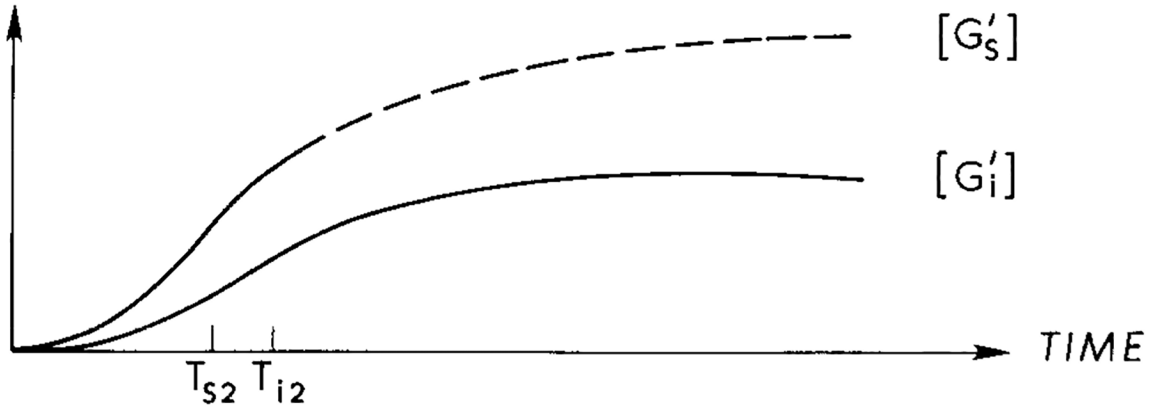

(b)

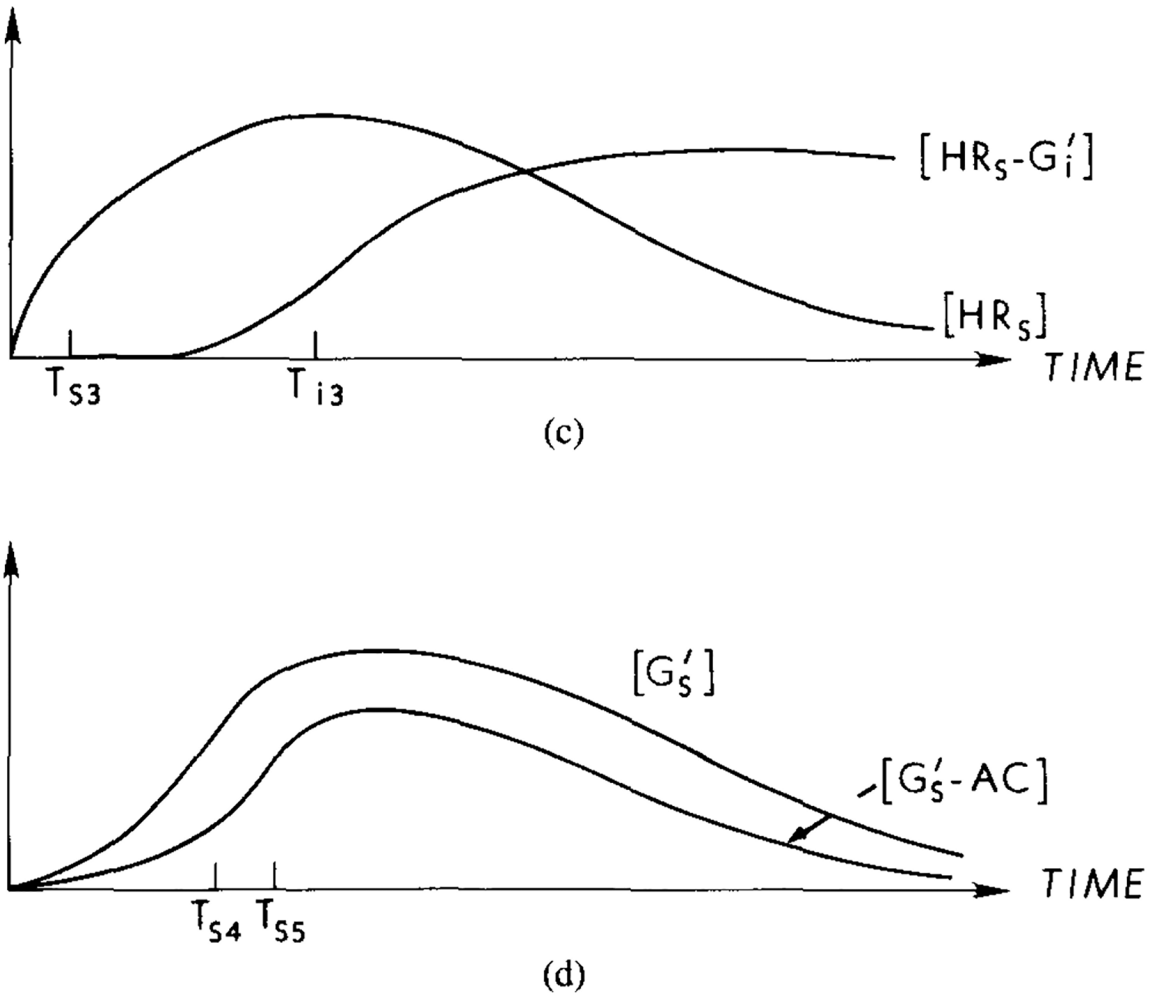

FIG. 4.

A qualitative description of latency and adaptation in the signal transduction process under a constant stimulus. The time for activation of G protein is the major component of the latency between stimulus arrival and activation of the adenylate cyclase. Adaptation at the receptor level results from the interaction of G_i' with HR_s, which reduces the amount of activated G_s and cyclase. (a) Response curves for HR_s and HR_i under a constant stimulus. T_{s1} and T_{i1}, represent the half-maximal times for the respective components. The dashed line indicates the response for HR_s in the absence of an inhibitory effect. (b) Response curves for the concentrations of G_s' and G_i'. T_{s2} and T_{i2} represent the half-maximal times for the respective components. The dashed line indicates the response if the inhibitory effect is not present. (c) In the presence of G_i', HR_s is diminished due to the formation of HR_sG_i'. The half-maximal time, T_{s3}, for HR_s in the presence of G_i' is approximately the same as T_{s1}, whereas $T_{i3} > T_{i2}$. (d) Response curves for the concentration of G_s' and $G_s'AC$. The half-maximal time for G_s', T_{s4}, is approximately equal to T_{s2}, whereas the half-maximal time for $G_s'AC$, T_{s5}, is greater than T_{s4}. The rate of $cAMP_i$ production is proportional to the concentration of G_sAC.

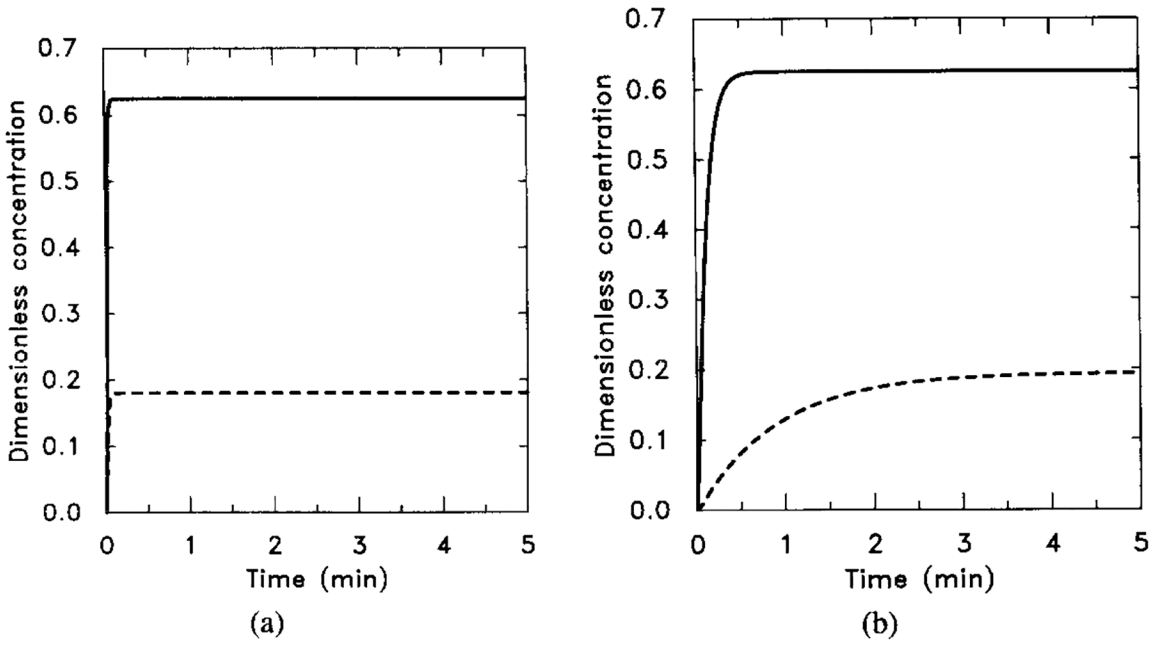

FIG. 5.

The response of the uncoupled system. The stimulus is [H] = 0.1 μM for $t \in (0, 5)$. The numerical results can be compared with the analytical results obtained from the analysis in Section 4 and with Figure 6 to verify the steady-state additivity of the uncoupled system. (a) The dimensionless concentrations of HR_s (solid line) and HR_i (dashed line). (b) The dimensionless concentrations of G'_s (solid line) and G'_i (dashed line). Note that the half-time for the buildup of G'_i agrees well with the theoretical estimate but that the rise time for G'_s is longer than the theoretical estimate. This discrepancy indicates that the pseudo-steady-state hypothesis applied to $[HR_sG_s]$ is probably not valid on this time scale.

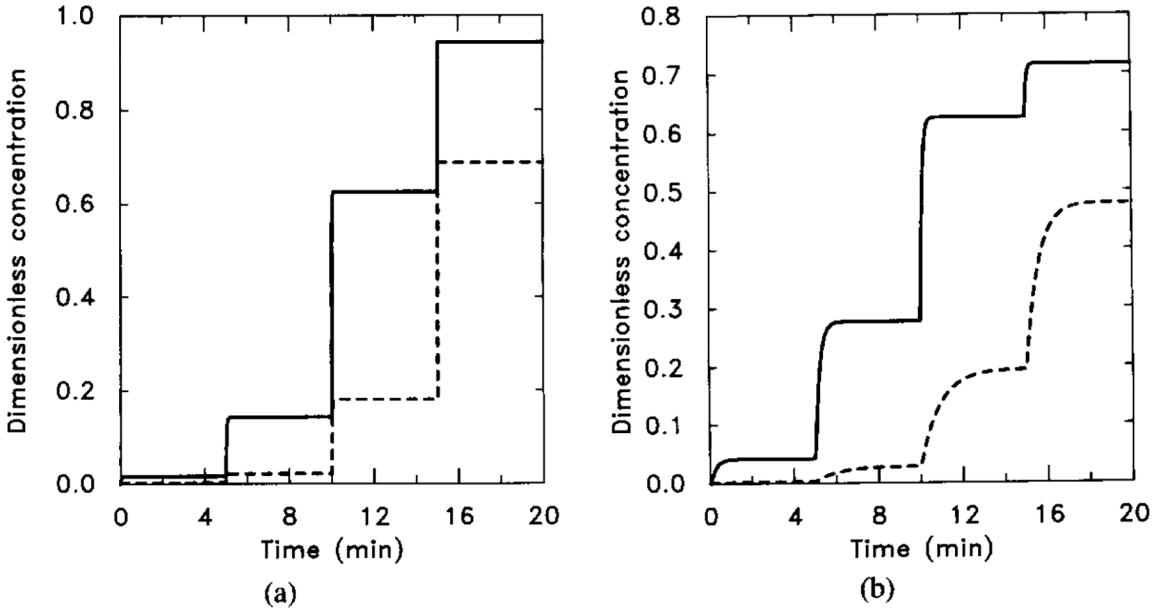

FIG. 6.

The response of the uncoupled system to sequential increases of the stimulus. The sequence is [H] = 0.001 μM for $t \in (0, 5)$; [H] = 0.001 μM for $t \in (5, 10)$; [H] = 0.1 μM for $t \in (10, 15)$; and [H] = 1.0 μM for $t \in (15, 20)$. (a) The dimensionless concentrations of HR_s (solid line) and HR_i (dashed line). (b) The dimensionless concentrations of G'_s (solid line) and G'_i (dahsed line).

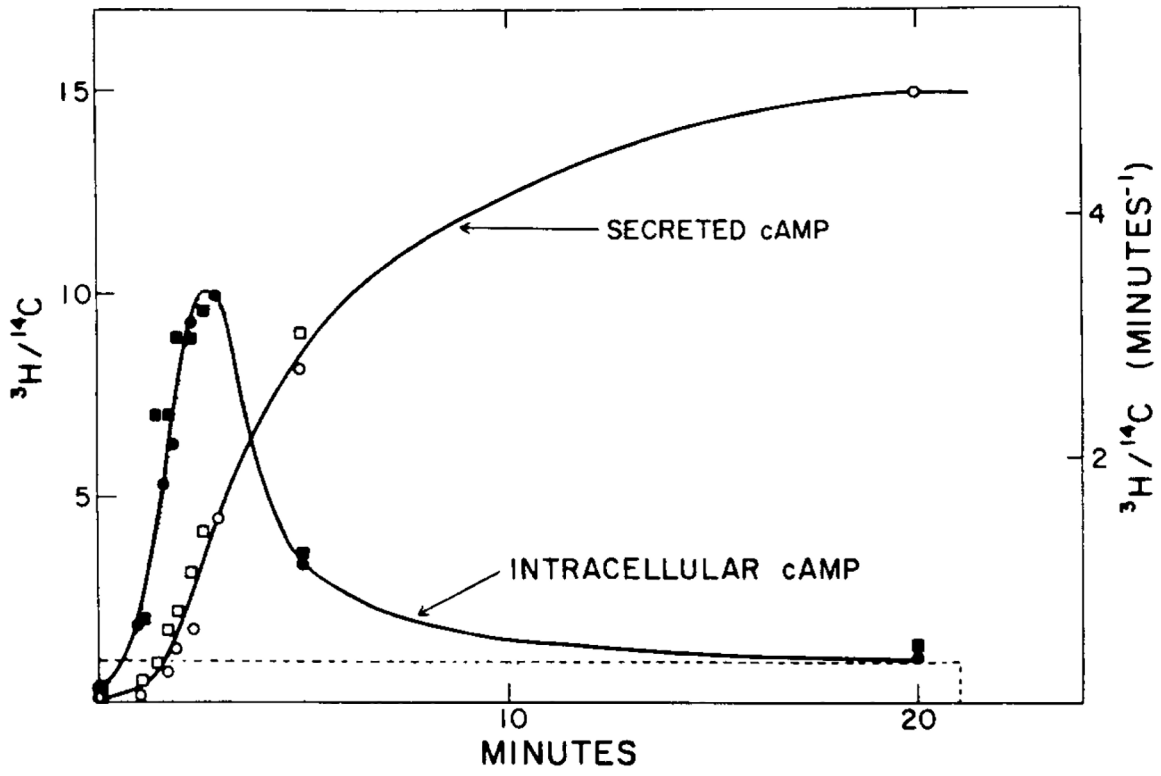

FIG. 7.

The experimental response of cAMP secretion to a single prolonged stimulus of 10^{-6} M extracellular cAMP (from [11]). The stimulus is a 20-min step function of 1 μM magnitude (dashed line). Two experimental results (circles and squares) are shown here for intracellular cAMP concentration (filled symbols) and cAMP secretion (open symbols).

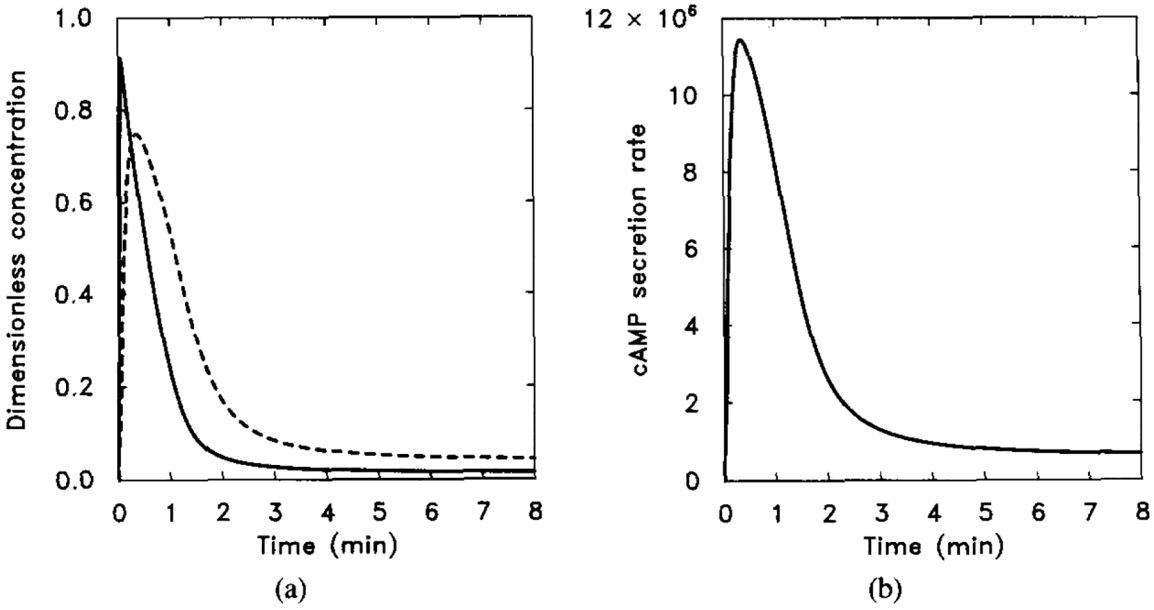

FIG. 8.

The response of the model to a prolonged stimulus of 10^{-6} M extracellular cAMP. The stimulus is [H] = 1.0 μM from $t = 0$ to $t = 8$ min. (a) The dimensionless concentrations of HR_S (solid line) and $cAMP_i/10$ (dashed line). (b) The dimensional secretion rate of $cAMP_i$ in molecules per cell per minute. Compare with Figure 7 for experimental data.

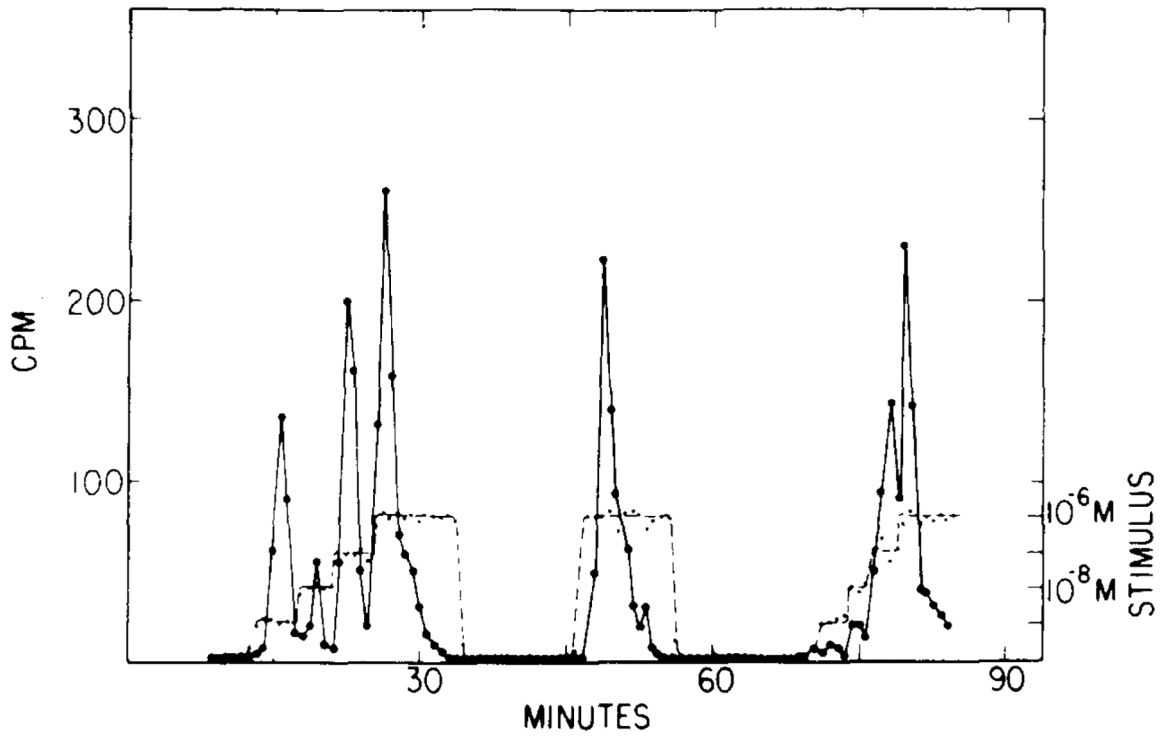

FIG. 9.

The experimentally observed cAMP secretion in response to a multistep stimulus. The first step is from 0 to 10^{-9} M, and this is followed by three 10-fold increases. (Adapted from [9].)

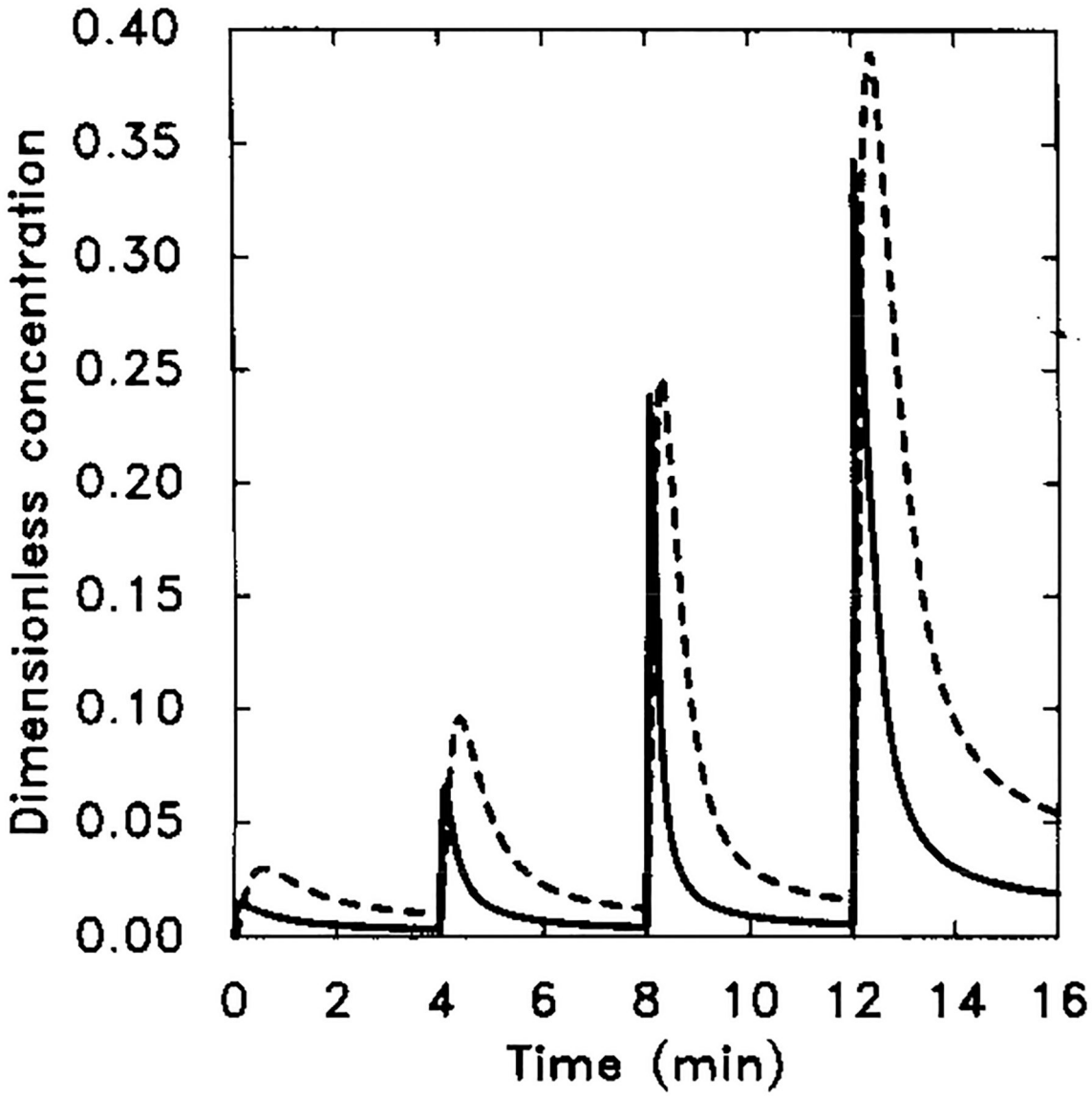

FIG. 10.

The numerical response of the system using the measured k_{-1}. Starting at $t = 0$ min, extracellular cAMP was increased from 0 to 10^{-9} M and then to 10^{-6} M in three 10-fold steps of 4 min duration. Dimensional parameter values are given in Table 4. The dimensionless concentrations of HR_s (solid line) and $cAMP_i/10$ (dashed line).

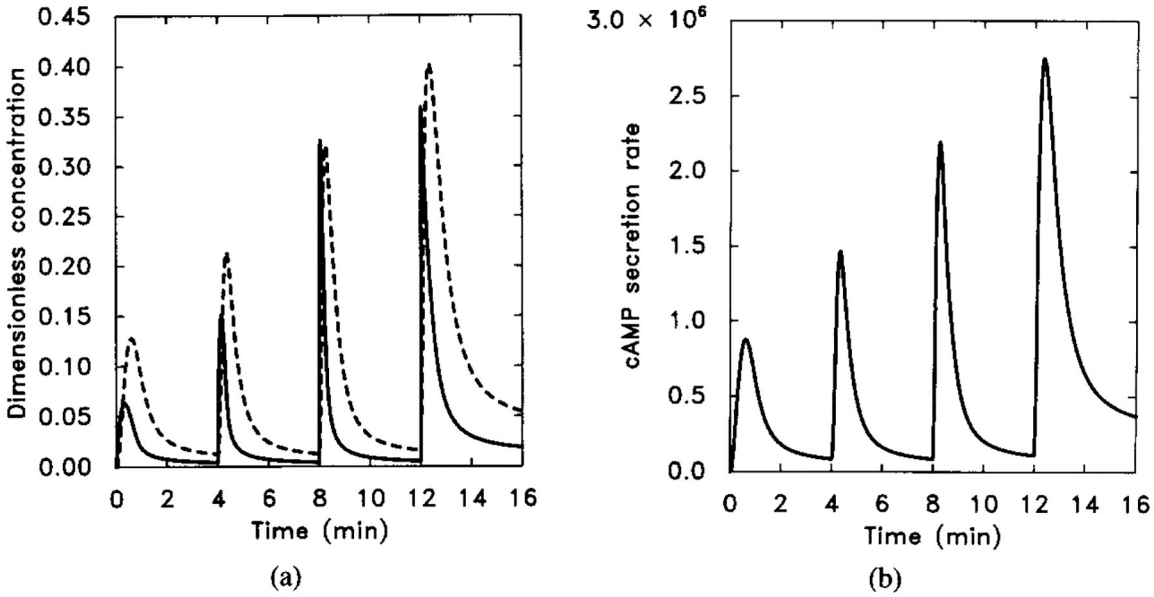

FIG. 11.

The numerical response to sequential 10-fold increases of stimuli with k_{-1} in Table 4 changed from 0.45 to 0.075. Other parameter values are unchanged. The stimulus is the same as in Figure 10. (a) The dimensionless concentrations of HR_s (solid line) and $cAMP_i/10$ (dashed line). (b) The dimensional secretion rate of $cAMP_i$ (molecules per cell per minute). Compare with Figure 9 for experimental data.

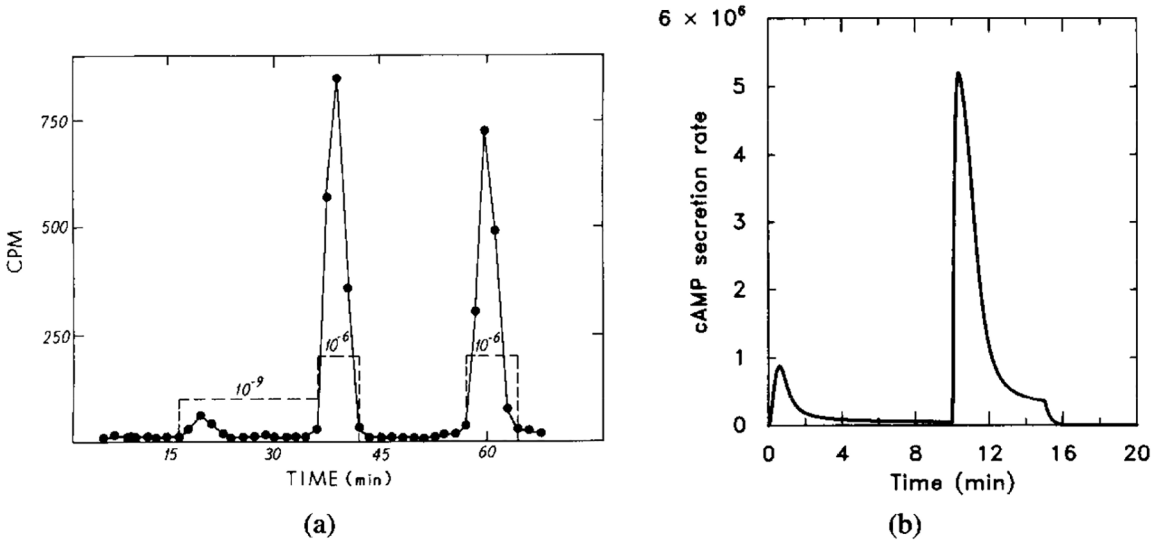

FIG. 12.

The experimental and model response to a two-step sequential stimulus. Note that after removal of the stimulus the unadapted portion decays very rapidly. The parameter value are the same as in Figure 11. The stimulus sequence is [H] = 10^{-9} M for $t = 0$ to $t = 10$, [H] = 10^{-6} M for $t = 10$ to $t = 15$, and [H] = 0 M for $t = 15$ to $t = 20$. (a) The experimentally observed response (adapted from [9]). (b) The dimensional secretion rate of $cAMP_i$ in molecules per cell per minute.

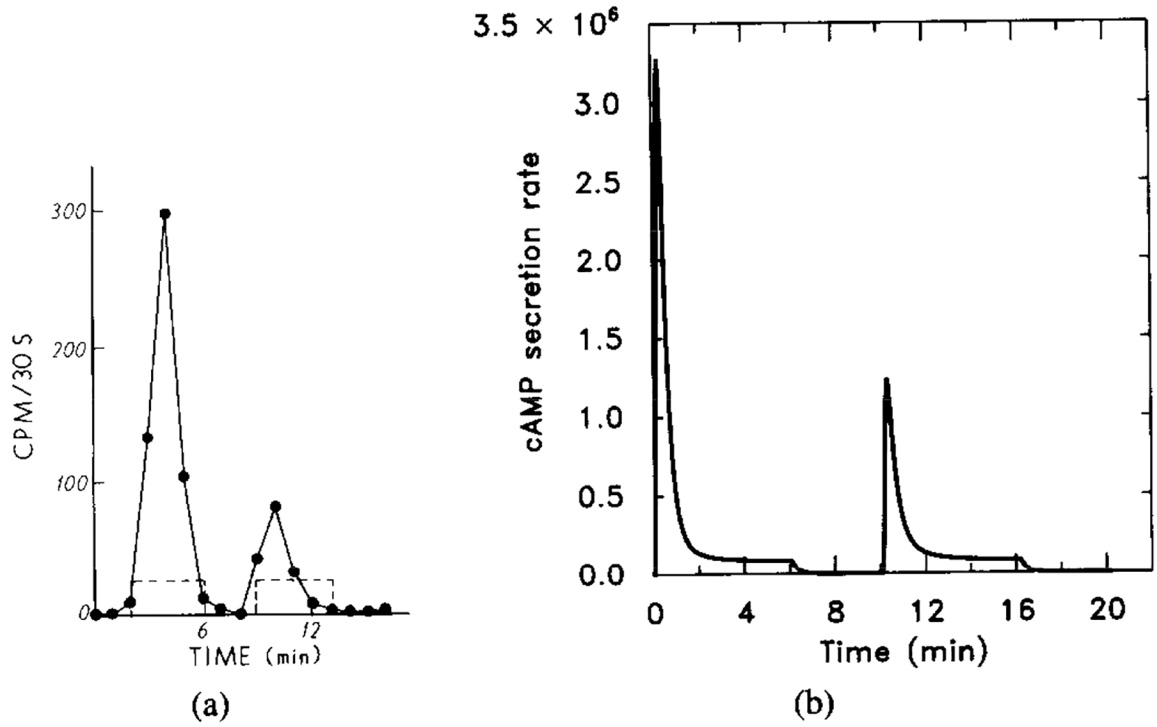

FIG. 13.

The experimental and numerical response to short two-step stimuli. The time course of the extracellular cAMP stimulus is 10^{-8} M (t = 0–6), 0 M (t = 6–10), 10^{-8} M (t = 10–16), and 0 M (t = 16–20). This experiment probes the time course of deadaptation, because the magnitude of the response to the second stimulus depends upon the degree to which the cells have recovered from the first stimulus. Parameter values are the same in Figure 11. (a) Experimental results (adapted from [11]). (b) The dimensional secretion rate of $cAMP_i$ (molecules per cell per minute). The response to the second signal of the same magnitude is much smaller because G_i' has not decayed completely. The magnitude of the second response increases with the elapsed time since the preceding signal.

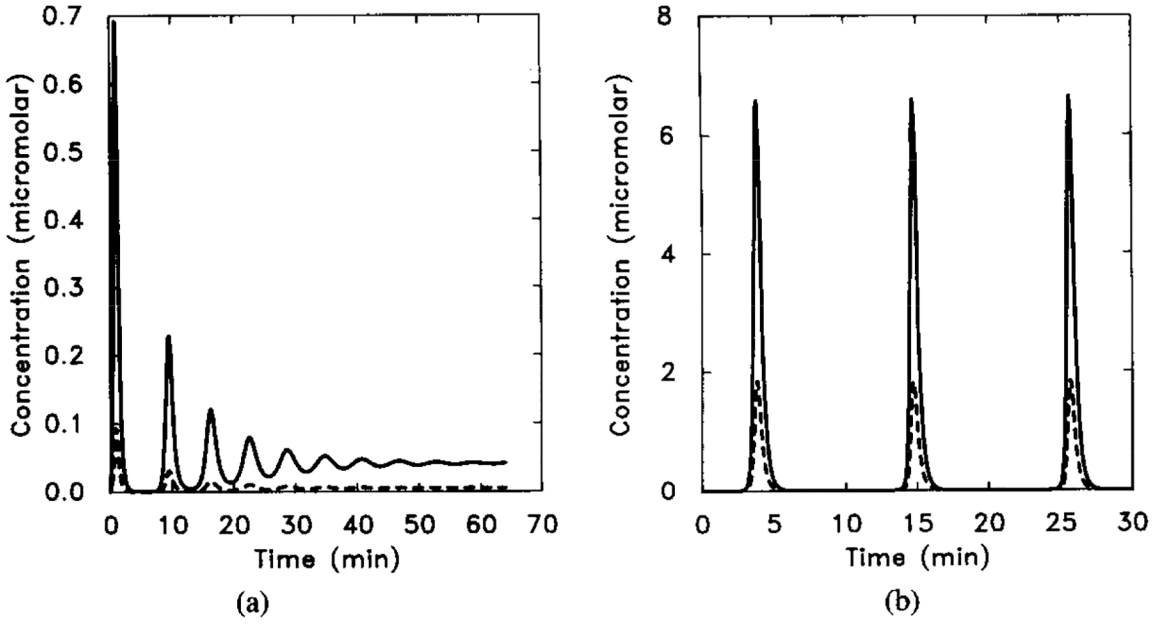

FIG. 14.

The dimensionless [cAMP$_i$] as a function of time, illustrating decaying oscillations. Parameter values are taken from Tables 8 and 13. The initial stimulus is [H] = 10^{-8} M. In this figure we scale both γ_2 and γ_5 by a factor f. Here $\gamma_2 = f \times 0.048$, and $\gamma_5 = f \times 0.224$, with $f = 5.0$. (b) A stable oscillation for $f = 10.0$. Shown are the dimensional intracellular cAMP concentration [cAMP$_i$] (solid line) and 10 times the extracellular cAMP concentration [cAMP$_o$] (dashed line).

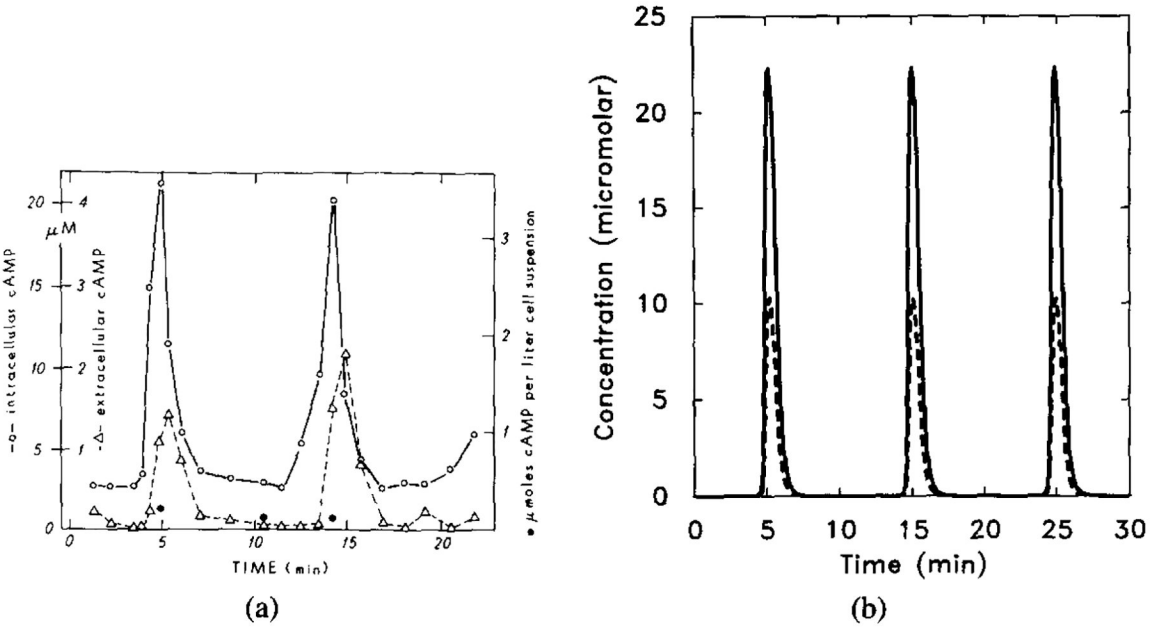

FIG. 15.

The experimental results for oscillations in suspensions and the corresponding numerical results. Parameter values are the same as in Figure 14 except $f = 25.0$. (a) Experimental measurements of intracellular (◯) and extracellular (Δ). Redrawn from Figure 2 of Gerisch and Wick [20]. (b) Dimensional intracellular cAMP concentration [$cAMP_i$] (solid line) and five times the extracellular cAMP concentration [$cAMP_o$] (dashed line).

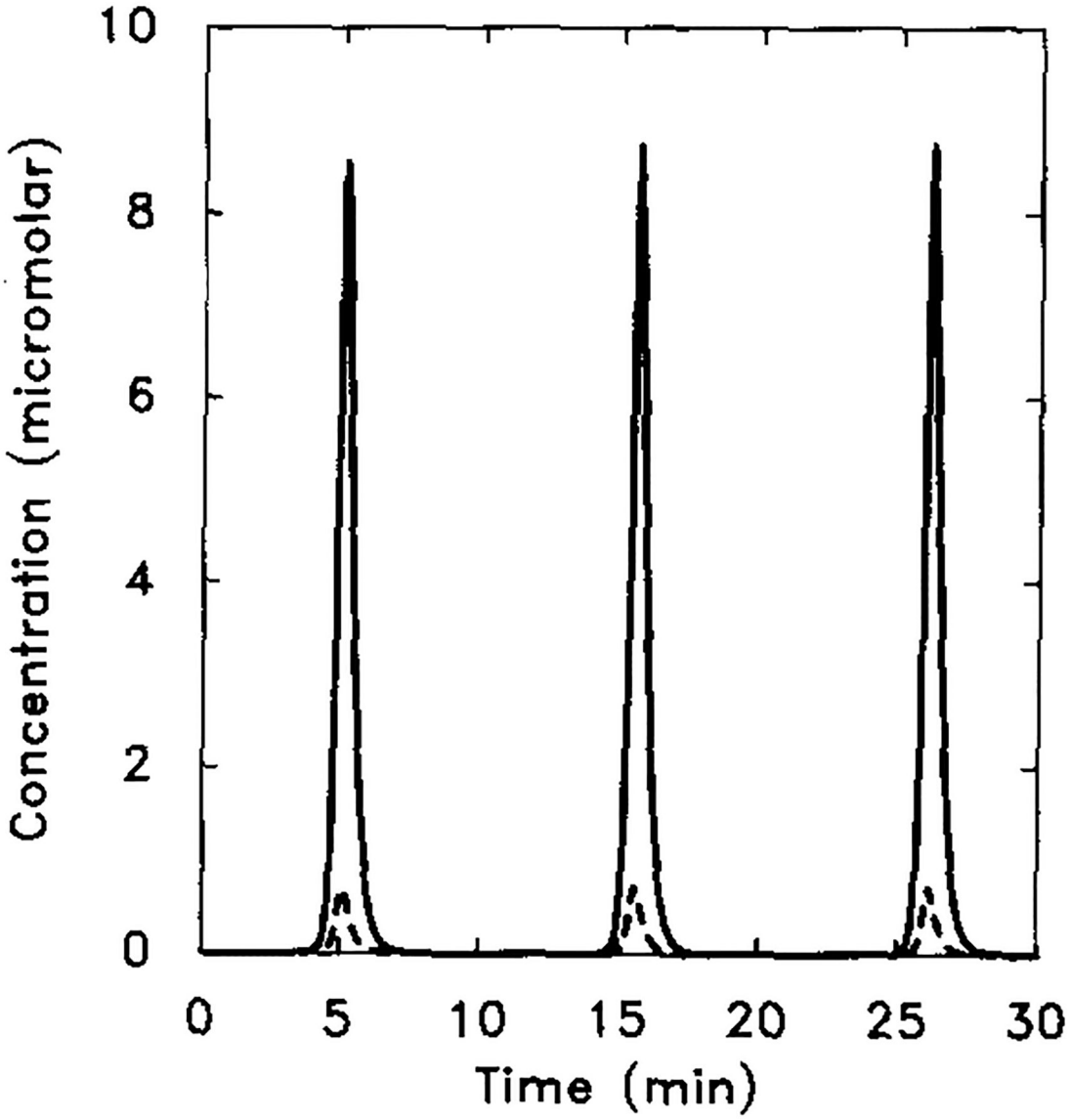

FIG. 16.

The magnitude of oscillation is significantly influenced by the parameters reflecting the activities of AC, iPDE, and mPDE. Here γ_6 is decreased by a factor of 10 ($\gamma_6 = 0.29$) and other parameter values are the same as in Figure 15. Shown are the dimensional intracellular cAMP concentration [$cAMP_i$] (solid line) and 10 times the extracellular cAMP concentration [$cAMP_o$] (dashed line).

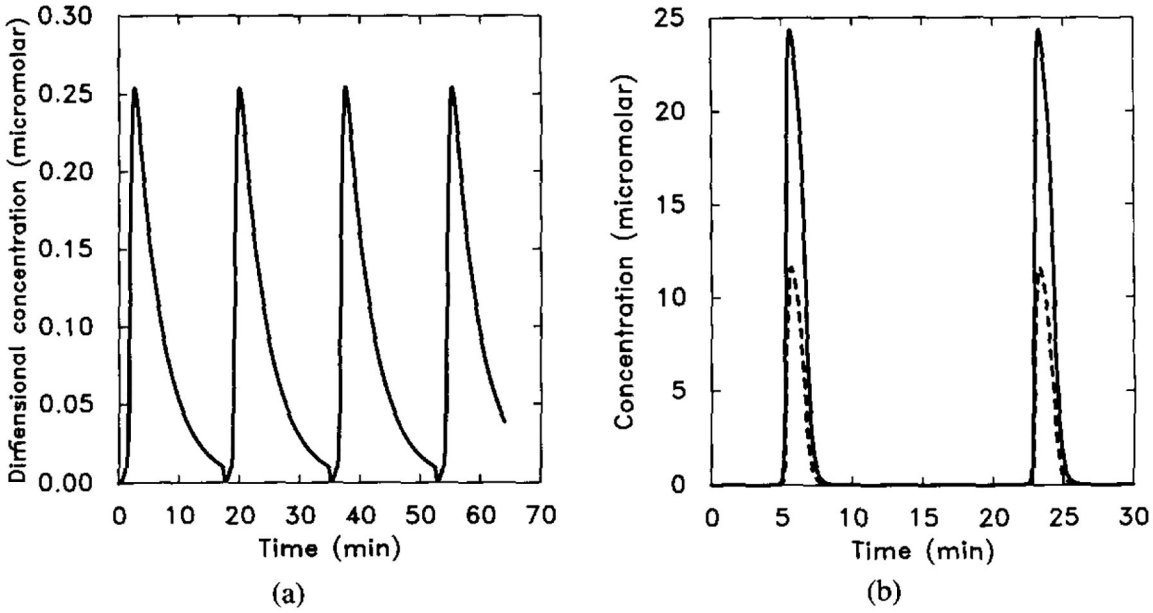

FIG. 17.

An illustration of how changes in β_2 and β_5 significantly change the oscillation frequency. Here β_2 and β_5 are divided by a factor of 2. Other parameter values are the same as in Figure 15. Compare with Figure 15. (a) The dimensionless concentration of G_i'. (b) Five times the intracellular cAMP concentration [$cAMP_i$] (solid line) and the extracellular cAMP concentration [$cAMP_o$] (dashed line).

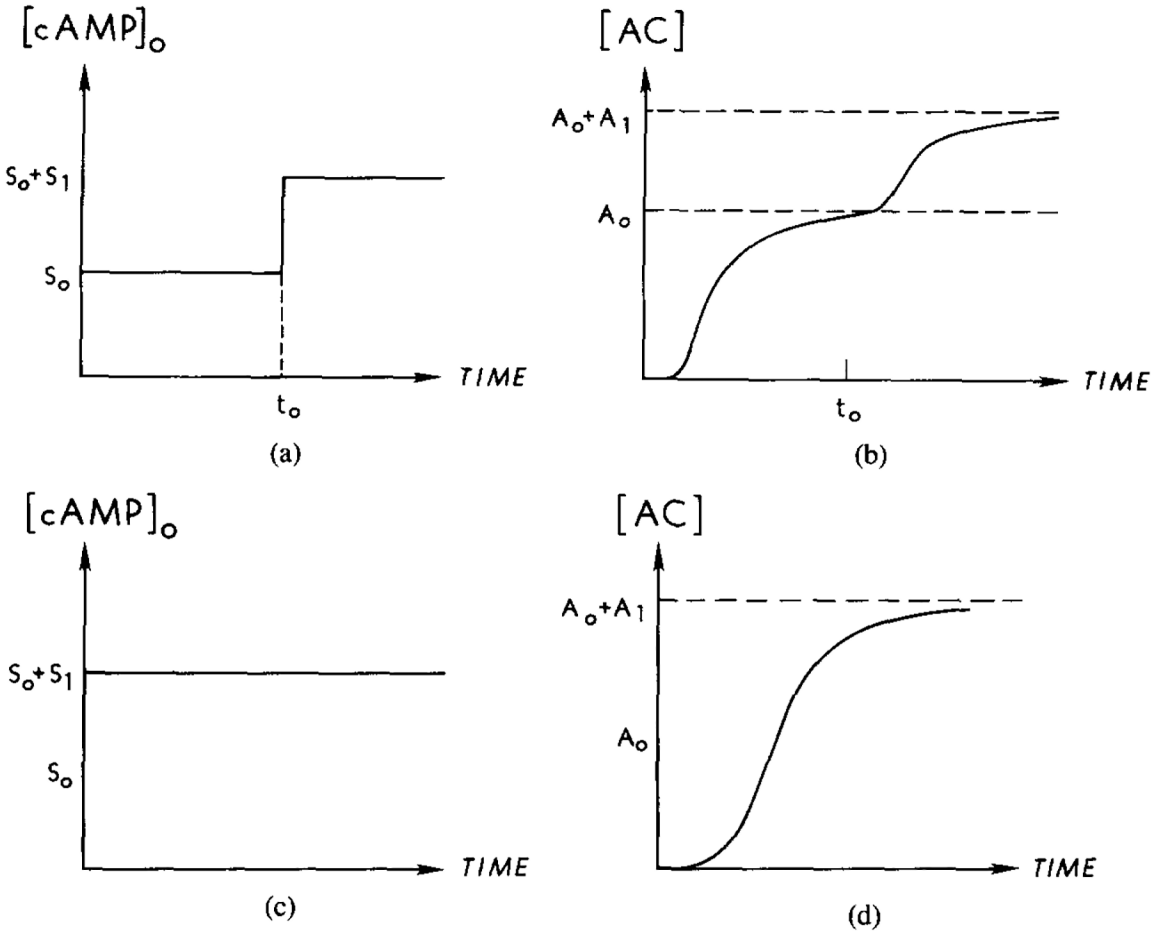

FIG. 18.

The steady-state additivity of cAMP production in the response to an extracellular cAMP signal, predicted for cholera toxin–treated cells. The steady-state concentration should depend only on the final stage of extracellular stimulus and not on the stimulus history. (a) A two-step stimulus of magnitude from S_0 to $S_0 + S_1$. (b) The corresponding response of activated adenylate cyclase to the stimulus in (a). The steady-state concentration should be from A_0 to $A_0 + A_1$. (c) A single-step stimulus of magnitude $S_0 + S_1$. (d) The corresponding response of activated adenylate cyclase to the stimulus in (c).

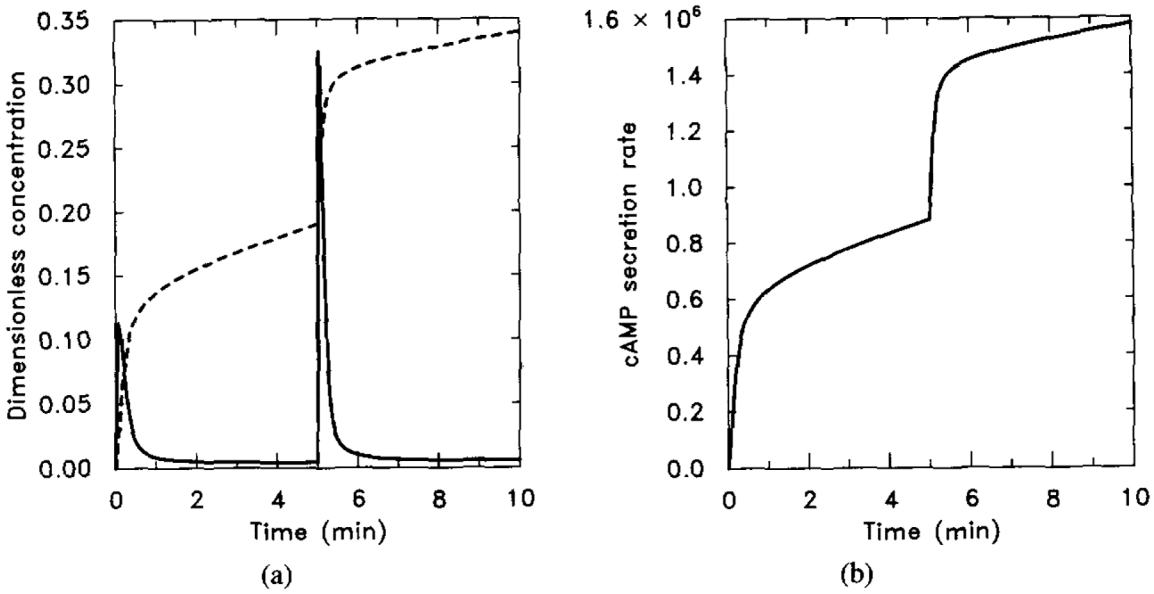

FIG. 19.

The effect of cholera toxin as predicted by the model. The result should be compared with Figure 18 to see the steady-state additivity. Parameter values are given in Table 4 with $k_5 = 0$ to mimic the effect of cholera toxin. The stimulus is 10^{-8} M for $t \in (0, 5)$ and 10^{-7} M for $t \in (5, 10)$. (a) Dimensionless concentrations of HR_s (solid line) and $cAMP_i/10$ (dashed line). (b) Dimensional secretion rate of $cAMP_i$ (molecules per cell per minute).

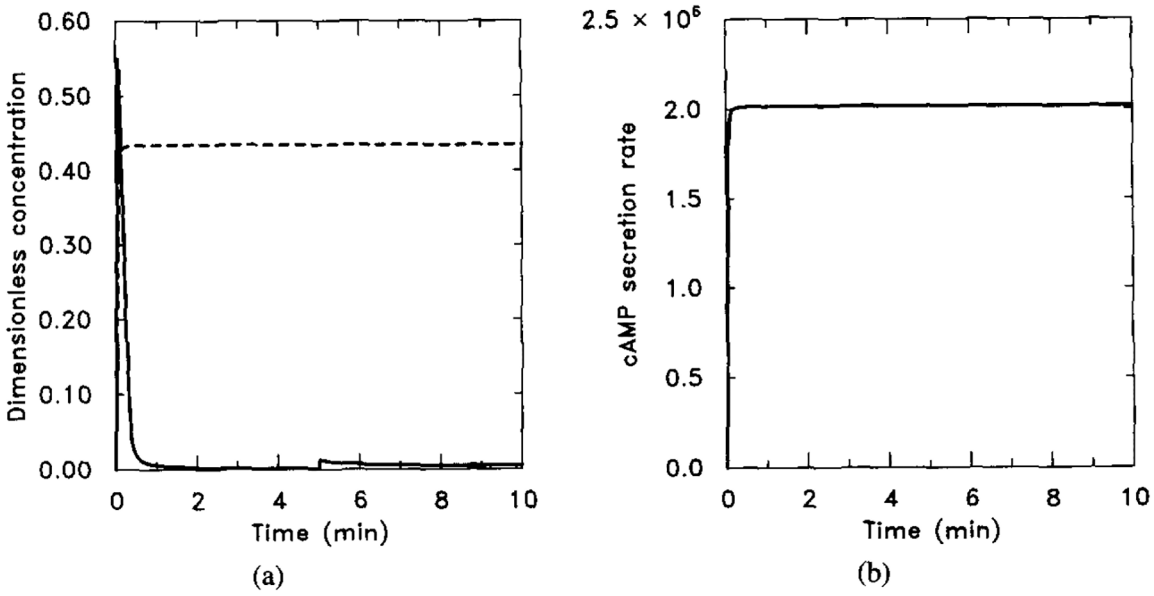

FIG. 20.

Numerical output for the experiment when GTP is replaced by GTPγS. The parameter values are the same as in Figure 19 with $h_5 = 0$ to simulate the fact that α_i-GTPγS is also nonhydrolyzable. The stimulus is 10^{-8} M for $t \in (0, 5)$ and 10^{-7} M for $t \in (5, 10)$. (a) Dimensionless concentrations of HR_s (solid line) and $cAMP_i/10$ (dashed line). (b) Dimensional secretion rate of $cAMP_i$ (molecules per cell per minute). (b) should be compared with (b) in Figure 19.

TABLE 1

The Variables and Their Symbols

Pathway	Species	Concentration	Meaning Function
Stimulus	HR_S	$y_1(t)$	Stimulus receptor bound with cAMP
	HR_SG_S	$y_2(t)$	cAMP-R_s complex bound with G_s
	G'_s	$y_3(t)$	Activated G_s protein
	G'_sAC	$y_4(t)$	Activated adenylate cyclase
	$\alpha_s GDP$	$y_5(t)$	Hydrolyzed G'_s
Inhibitory	HR_i	$y_6(t)$	Inhibitory receptor bound with cAMP
	HR_iG_i	$y_7(t)$	cAMP-R; complex bound with G_i
	G'_i	$y_8(t)$	Activated G_i protein
	$HR_sG'_i$	$y_9(t)$	Activated G_i bound with HR_S
	$\alpha_i GDP$	$y_{10}(t)$	Hydrolyzed G'_i
Generation and secretion	$G'_sAC - ATP$	$y_{11}(t)$	Activated AC bound with ATP
	$cAMP_i$	$y_{12}(t)$	Intracellular cAMP
	$iPDE\text{-}cAMP_i$	$y_{13}(t)$	Intracellular iPDE-cAMP complex
	$cAMP^*_o$	$y^*_{14}(t)$	Total amount of secreted cAMP

TABLE 2

The Quantities Determined by Conservation Conditions

Species	Concentration	Definition
R_s	$z_1(t)$	Free R_s in membrane
G_s	$z_2(t)$	Free G_s in membrane
UC	$z_3(t)$	Free adenylate cyclase in the membrane
R_i	$z_4(t)$	Free R_i in the membrane
G_i	$z_5(t)$	Free G_i in the membrane
$\beta\gamma$	$z_6(t)$	Free $\beta\gamma$ subunits in the membrane
iPDE	$z_7(t)$	Free PDE in the cytoplasm

TABLE 3

Bounds for the Independent and Dependent Dimensional Variables

$0 \leqslant y_1 \leqslant [\mathrm{R_s}]_T$	$0 \leqslant y_8 \leqslant [\mathrm{G_i}]_T$	$0 \leqslant z_1 \leqslant [\mathrm{R_s}]_T$
$0 \leqslant y_2 \leqslant \min([\mathrm{R_s}]_T, [\mathrm{G_s}]_T)$	$0 \leqslant y_9 \leqslant \min([\mathrm{R_s}]_T, [\mathrm{G_s}]_T)$	$0 \leqslant z_2 \leqslant [\mathrm{G_s}]_T$
$0 \leqslant y_3 \leqslant [\mathrm{G_s}]_T$	$0 \leqslant y_{10} \leqslant [\mathrm{G_i}]_T$	$0 \leqslant z_3 \leqslant [\mathrm{UC}]_T$
$0 \leqslant y_4 \leqslant \min([\mathrm{G_s}]_T, [\mathrm{UC}]_T)$	$0 \leqslant y_{11} \leqslant \min([\mathrm{G_s}]_T, [\mathrm{UC}]_T)$	$0 \leqslant z_4 \leqslant [\mathrm{R_i}]_T$
$0 \leqslant y_5 \leqslant [\mathrm{G_s}]_T$	$0 \leqslant y_{12} \leqslant \infty$	$0 \leqslant z_5 \leqslant [\mathrm{G_i}]_T$
$0 \leqslant y_6 \leqslant [\mathrm{R_i}]_T$	$0 \leqslant y_{13} \leqslant [\mathrm{iPDE}]_T$	$0 \leqslant z_6 \leqslant [\mathrm{G_s}]_T + [\mathrm{G_i}]_T$
$0 \leqslant y_7 \leqslant \min([\mathrm{R_i}]_T, [\mathrm{G_i}]_T)$	$0 \leqslant y_{14}^* \leqslant \infty$	$0 \leqslant z_7 \leqslant [\mathrm{iPDE}]_T$

TABLE 4

Estimates of the Kinetic Parameters

Pathway	Parameter	Estimated value	Source
Stimulus	k_1	7.5 s^{-1} μM^{-1}	van Haastert and de Wit [49]
	k_{-1}	0.45 s^{-1}	van Haastert and de Wit [49]
	k_2	1.0×10^3 $m^2/(\mu mol \cdot s)$	Gilman [21]
	k_{-2}	0.0 s^{-1}	Gilman [21]
	k_3	1.0×10^3 s^{-1}	Gilman [21]
	k_4	1.0×10^4 $m^2/(\mu mol \cdot s)$	
	k_{-4}	0.0 s^{-1}	
	k_5	0.0625 s^{-1}	Gilman [21]
	k_6	1.0×10^5 $m^2/(\mu mol \cdot s)$	
Inhibitory	h_1	2.2 s^{-1} μM^{-1}	van Haastert and de Wit [49]
	h_{-1}	1.0 s^{-1}	van Haastert and de Wit [49]
	h_2	40.0 $m^2/(\mu mol \cdot s)$	Dinauer et al. [13]
	h_{-2}	0.0 s^{-1}	Dinauer et al. [13]
	h_3	4.0×10^2 s^{-1}	Dinauer et al. [13]
	h_4	5.0×10^6 $m^2/(\mu mol \cdot s)$	
	h_{-4}	0.0 s^{-1}	
	h_5	7.5×10^{-3} s^{-1}	Gerisch and Wick [20]
	h_6	17.0 s^{-1}	van Haastert and de Wit [49]
	h_7	10^5 $m^2/(\mu mol \cdot s)$	
cAMP generation and secretion	l	20.2 s^{-1}	Levitzki [29]
	l_{-1}	20.2 s^{-1}	Levitzki [29]
	l_2	202 s^{-1}	Levitzki [29]
	l_3	5.0×10^{-4} $m^3/(\mu mol \cdot s)$	Rapp et al. [37]
	l_{-3}	0.0 s^{-1}	Rapp et al. [37]
	l_4	50 s^{-1}	Rapp et al. [37]
	l_5	0.157 s^{-1}	

TABLE 5

Estimates for the Fixed Concentrations

Quantity conserved	Molecules per cell	Standard concentration
$[R_s]_T$, $[G_s]_T$, $[UC]_T$	3.84×10^4	1.67×10^{-4} μmol/m^2
$[R_i]_T[G_i]_T$	5.76×10^4	2.50×10^{-4} μmol/m^2
$[iPDE]_T$	7.28×10^5	1.73×10^3 μmol/m^3

TABLE 6

The Relationship Between Dimensional and Dimensionless Variables

	Species	Dimensional form	Dimensionless form
Stimulus pathway	HR_S	y_1	$u_1 = y_1/[R_s]_T$
	HR_SG_S	y_2	$v_1 = \frac{k_{-2}+k_3}{k_2[R_s]_T[G_s]_T}y_2$
	G'_s	y_3	$u_2 = y_3/[G_s]_T$
	G'_sAC	y_4	$u_3 = y_4/[UC]_T$
	$\alpha_s GDP$	y_5	$v_2 = (k_6/k_5)y_5$
Inhibitory pathway	HR_i	y_6	$u_4 = y_6/[R_i]_T$
	HR_iG_i	y_7	$v_3 = \frac{h_{-2}+h_3}{h_2[R_i]_T[G_i]_T}y_7$
	G'_i	y_8	$u_5 = y_8/[G_i]_T$
	$HR_sG'_i$	y_9	$u_5 = y_8/[G_i]_T$
	$\alpha_i GDP$	y_{10}	$v_4 = (h_7/h_5)y_{10}$
cAMP generation and secretion	$G'_sAC - ATP$	y_{11}	$v_5 = \frac{l_{-1}+l_2}{l_1[UC]_T}y_{11}$
	$cAMP_i$	y_{12}	$u_7 = y_{12}/[iPDE]_T$
	$iPDE\text{-}cAMP_i$	y_{13}	$v_6 = (l_{-3}+l_4)y_{13}/l_3[iPDE]_T^2$
	$cAMP^*_o$	y^*_{14}	$u^*_8 = y^*_{14}/[iPDE]_T$
Time scale		t	$\tau = k_5 t$

TABLE 7

The Small Dimensionless Kinetic Parameters and Their Values

Small parameter	Relation to dimensional parameters	Value
ϵ_1	$k_5/(k_{-2} + k_3)$	6.25×10^{-5}
ϵ_2	$k_5/k_6[G_s]_T$	3.74×10^{-4}
ϵ_3	$k_5/(h_{-2} + h_3)$	1.56×10^{-4}
ϵ_4	$k_5/h_7[G_i]_T$	2.50×10^{-4}
ϵ_5	$k_5/(l_{-1} + l_2)$	2.81×10^{-4}
ϵ_6	$k_5/(l_{-3} + l_4)$	1.56×10^{-3}

TABLE 8

Other Dimensionless Parameters and Their Values

	Dimensionless parameter	Relation to dimensional parameter	Value
Stimulus Pathway	a_H	$(k_1/k_5)H(t)$	120 $\mu M^{-1} \times H(t)$
	a_1	k_{-1}/k_5	7.2
	a_2	$k_2[G_s]_T/k_5$	2.67
	a_3	$k_3/(k_{-2} + k_3)$	1.0
	a_4	$k_4[G_s]_T/k_5$	26.7
Inhibitory Pathway	β_H	$(h_1/k_5)H(t)$	35.2 $\mu M^{-1} \times H(t)$
	β_1	h_{-1}/k_5	16.0
	β_2	$h_2[G_i]_T/k_5$	0.16
	β_3	$h_3/(h_{-2} + h_3)$	1.0
	β_4	$h_4[G_i]_T/k_5$	2.0×10^4
	β_5	h_5/k_5	0.12
	β_6	h_6/k_5	272.0
cAMP generation and secretion	γ_1	l_1/k_5	323.2
	γ_2	$\frac{l_2[UC]_T}{(l_{-1} + l_2)[iPDE]_T}$	0.048
	γ_3	$(L_{-3} + l_4)/l_3[iPDE]_T$	57.7
	γ_4	l_4/k_5	800.0
	γ_5	l_5/k_5	0.224
Independent concentrations	c_1	$[R_s]_T/[G_s]_T$	1.0
	c_2	$[R_i]_T/[G_i]_T$	1.0
	c_3	$[R_s]_T/[G_i]_T$	0.668
Dependent concentrations	c_4	$[UC]_T/[G_s]_T$	1.0
	c_1/c_3	$[G_i]T/[G_s]_T$	1.5

TABLE 9

Bounds for the Dimensionless Variables

Nonsingular variable	Singular variable
$0 \leqslant u_1 \leqslant 1$	$0 \leqslant v_1 \leqslant \min\left(\frac{k_{-2}+k_3}{k_2[\mathrm{R_s}]_T}, \frac{k_{-2}+k_3}{k_2[\mathrm{G_s}]_T}\right)$
$0 \leqslant u_2 \leqslant 1$	$0 \leqslant v_2 \leqslant k_6[\mathrm{G_s}]_T/k_5$
$0 \leqslant u_3 \leqslant \min(1, [\mathrm{G_s}]_T/[\mathrm{UC}]_T)$	$0 \leqslant v_3 \leqslant \min\left(\frac{h_{-2}+h_3}{h_2[\mathrm{R_i}]_T}, \frac{h_{-2}+h_3}{h_2[\mathrm{G_i}]_T}\right)$
$0 \leqslant u_4 \leqslant 1$	$0 \leqslant v_4 \leqslant h_7[\mathrm{G_i}]_T/h_5$
$0 \leqslant u_5 \leqslant 1$	$0 \leqslant v_5 \leqslant \min\left(\frac{l_{-1}+l_2}{l_1}, \frac{(l_{-1}+l_2)[\mathrm{G_s}]_T}{l_1[\mathrm{UC}]_T}\right)$
$0 \leqslant u_6 \leqslant \min(1,[\mathrm{G_i}]_T/[\mathrm{R_s}]_T)$	$0 \leqslant v_6 \leqslant (l_{-3}+l_4)/l_3[\mathrm{iPDE}]_T$
$0 \leqslant u_7 \leqslant \infty$	$0 \leqslant u_8^* \leqslant \infty$

TABLE 10

The steady-state response of uncoupled stimulus and inhibitory pathways to external cAMP stimuli

[H](μM)	10^{-4}	10^{-3}	10^{-2}	10^{-1}	1	10
$\frac{[HR_S]_s}{[R_S]_T} \times 100$	0.17%	1.64%	14.3%	62.5%	94.0%	99.4%
$\frac{[HR_i]_s}{[R_i]_T} \times 100$	0.022%	0.22%	2.15%	18%	69.0%	95.7%
$\frac{[G'_s]_s}{[G_s]_T} \times 100$	0.45%	4.36%	27.7%	62.6%	71.5%	72.7%
$\frac{[G'_i]_s}{[G_i]_T} \times 100$	0.03%	0.29%	2.79%	19.4%	47.9%	57.1%

TABLE 11

The Steady-State Concentrations of Components in the Transduction Steps

[H] (μM)	10^{-4}	10^{-3}	10^{-2}	10^{-1}	1	10
$\frac{[HR_i]_S}{[R_i]_T} \times 100$	0.022%	0.22%	2.15%	18.0%	69.0%	95.7%
$\frac{[G'_i]^*_s}{[G_i]_T} \times 100$	0.03%	0.29%	2.79%	19.4%	47.9%	57.1%
$\frac{[HR_s]_s}{[R_s]_T} \times 100$	0.093%	0.18%	0.21%	0.30%	1.01%	4.33%
$\frac{[G'_s]^*_s}{[G_s]_T} \times 100$	0.03%	0.058%	0.067%	0.096%	0.32%	1,37%

TABLE 12

Additional Dimensionless Variables and Parameters

Parameters	Parameters	Variables
$\alpha_0 = \frac{k_1[\text{iPDE}]_T}{k_5}$	$\gamma_8 = \frac{l_{-8} + l_9}{l_8[\text{iPDE}]_T}$	$v_7 = \frac{(l_{-6} + l_7)y_{15}}{l_6[\text{iPDE}]_T[\text{mPDE}]_T}$
$\beta_0 = \frac{h_1[\text{iPDE}]_T}{k_5}$	$\gamma_9 = \frac{l_9[\text{ePDE}]_T}{k_5[\text{iPDE}]_T}$	$v_8 = \frac{(l_{-8} + l_9)y_{16}}{l_8[\text{iPDE}]_T[\text{ePDE}]_T}$
$\gamma_6 = \frac{(l_{-6} + l_7)}{l_6[iPDE]_T}$	$\epsilon_7 = \frac{k_5}{(l_{-6} + l_7)}$	
$\gamma_7 = \frac{l_7[mPDE]_T A_c}{k_5[iPDE]_T V_c}$	$\epsilon_8 = \frac{k_5}{(l_{-8} + l_9)}$	

TABLE 13

Estimated Values for the New Dimensionless Parameters

$\alpha_0 = 208.0$	$\gamma_6 = 2.9$	$\gamma_8 = 4607$	$\rho = 0.14$
$\beta_0 = 61.0$	$\gamma_7 = 225.4$	$\gamma_9 = 659.3$	